Annu. Rev. Physiol. 2006. 68:507–41
doi: 10.1146/annurev.physiol.68.072304.114110

First published online as a Review in Advance on October 31, 2005

STRESS TRANSMISSION IN THE LUNG: Pathways from Organ to Molecule

Jeffrey J. Fredberg[1] and Roger D. Kamm[2]
[1]*Department of Environmental Health, Harvard School of Public Health, Boston, Massachusetts 02115; email: jfredber@hsph.harvard.edu*
[2]*Department of Mechanical Engineering, Massachusetts Institute of Technology, Cambridge, Massachusetts 02139; email: rdkamm@mit.edu*

Key Words force, pressure, remodeling, stretch, tension, cytoskeleton, focal adhesion, airway, alveolus

■ **Abstract** Gas exchange, the primary function of the lung, can come about only with the application of physical forces on the macroscale and their transmission to the scale of small airway, small blood vessel, and alveolus, where they serve to distend and stabilize structures that would otherwise collapse. The pathway for force transmission then continues down to the level of cell, nucleus, and molecule; moreover, to lesser or greater degrees most cell types that are resident in the lung have the ability to generate contractile forces. At these smallest scales, physical forces serve to distend the cytoskeleton, drive cytoskeletal remodeling, expose cryptic binding domains, and ultimately modulate reaction rates and gene expression. Importantly, evidence has now accumulated suggesting that multiscale phenomena span these scales and govern integrative lung behavior.

INTRODUCTION

This review deals with mechanical stress in the lung at the levels of tissue, cell, and molecule. Our goal is to elucidate biophysical mechanisms that underlie mechanical function at each of these levels, the connections between levels, and their alterability in selective but biologically important departures from the normal state. There are many excellent reviews of lung mechanics on the macroscale (1, 2) and the microscale (3), but for the pulmonary cell biologist that literature may be to some extent unfamiliar, and many of its underlying concepts may not be readily accessible. More importantly, we know of no review that emphasizes the pathway for transmission of mechanical stresses from the pulmonary macroscale to the cell microenvironment, across the cell wall, through the cytoskeleton (CSK), and ultimately to the nucleus. This review is designed to fill that gap.

It is important to remember at the outset that the main function of the lung is gas exchange. For a long time biologists have sought to understand the pathway for oxygen delivery from the atmosphere, through the lung, across the air-blood

barrier, through the circulation, and, ultimately, to the mitochondria, where the oxygen is consumed. To achieve this feat the lung provides branching networks of conducting airways and blood vessels for air and blood to convect to the alveolar septum, and there they come into intimate contact. At that level the surface area is large, the distances are small, and therefore, the main mechanism of gas exchange is passive diffusion. "The pathway for oxygen" and its structure and function have come to be well understood and are summarized best in the text of the same name by Weibel (4).

The primary function of the lung may center on gas exchange, but there are other demands that must be simultaneously met. Some of these demands come into conflict with gas exchange and therefore lead to interesting questions of biological design. Coming to the forefront in that regard are mechanical considerations. More than anything else, the lung is a mechanical organ; the act of breathing is a mechanical process that entails the cyclic application of physical stresses at the pleural surface as well as the transmission of those stresses throughout the lung tissue and its complement of adherent cells. If strain is defined as the resulting length change of a structure per unit initial length, then in the course of a lifetime, the lung, as well as the cells within it, must withstand 10^9 strain cycles with amplitudes that approach 4% during quiet tidal breathing and 10^7 strain cycles with amplitudes that approach 25% during sighs, deep inspirations, or heavy exercise (5). By the standards of common engineering materials, these strains are extreme and would appear to call for tissue structures that are rather substantial. But at the same time, gas exchange is favored when the tissue diffusional barrier is minimal. To explain lung structure in the context of such competing demands, Taylor, Weibel, & Hoppeler (6, 7) introduced the principle of symmorphosis. Symmorphosis holds that at each level along the pathway for oxygen, there is enough structure, but just barely enough, to support the required oxygen flux. That is to say, in the biological design of the pathway for oxygen, there is little wasted structure and no overdesign. The closely related issues of the scaling of oxygen demand and oxygen transport with body size are treated in the excellent volumes by Schmidt-Nielson (8) and McMahon (9). In addition to supporting oxygen flux, the lung must provide the appropriate mechanical microenvironment for epithelial cells, endothelial cells, and the other 60 resident cell types in between, many of which sense and respond to mechanical stress or strain.

THE LUNG MICROENVIRONMENT AND ITS STATE OF STRESS

The lung is like a balloon that requires an externally generated distending stress to maintain its state of inflation; unlike most other organs, the lung is a pressure-supported structure (10–14). That distending stress is provided by the chest wall and associated muscles of respiration (15–19). At functional residual capacity, the

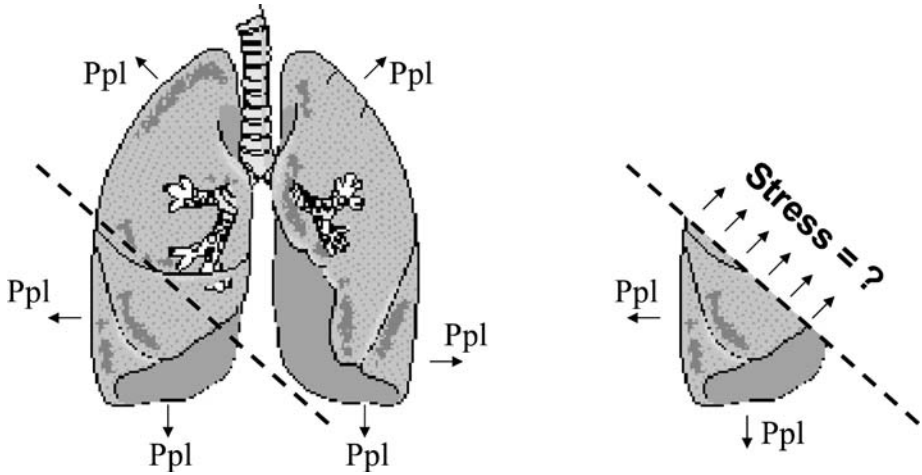

Figure 1 To remain in mechanical equilibrium, the normal (perpendicular) stress acting upon an imaginary cut surface must equal the pleural pressure (Ppl). Because pleural pressure is usually negative, arrows depicting that stress are shown as exerting a distending stress upon the visceral pleura.

lung is distended by an inflating pressure[1] of approximately 2–5 cm H_2O. That is, if the pressure at the airway opening, Pao, were atmospheric and the pressure in the pleural space, Ppl, were 5 cm H_2O below atmospheric, then the inflating pressure—also called the transpulmonary pressure (P_L)—would be 5 cm H_2O; at total lung capacity (TLC) the inflating pressure is approximately 30 cm H_2O. Because P_L = Pao – Ppl, lung-inflating pressure depends upon this pressure difference rather than either Pao or Ppl individually; as far as lung inflation and tissue distension are concerned, it makes no difference whether Pao is increased or Ppl is decreased. For example, during a Valsalva maneuver, Pao, alveolar pressure (P_A), and Ppl can approach 200 cm H_2O, whereas P_L changes hardly at all, merely decreasing slightly secondary to the small decrease of lung volume attributable to alveolar gas compression.

What is the state of distending stress within lung parenchymal tissues? The answer to this question is complicated, but we can make extremely good estimates of the average value of that stress. If we ignore for the moment the effects of gravity (20, 21), the lung is subjected on all of its outside surfaces to a pleural pressure that is roughly uniform (22). We imagine a plane cutting through the lung at an arbitrary position and angle, and then ask, what is the state of stress that must be acting on that imaginary cut face for the cut lung segment to remain in mechanical equilibrium (Figure 1)? Below, we deal with local variations of

[1]A note on units: 1 Pa $=$ 1 N m^{-2} $=$ 10 dynes cm^{-2} $=$ 1.033×10^{-2} cm H_2O.

stress at a finer level of resolution, but here we seek only a coarse-grained average that blurs all microstructural detail. Newton's third law requires that if the lung segment in question is not accelerating, then the sum of all forces acting upon it must be zero. As a result, the average stress acting on the cut face must be exactly the pleural pressure, although over that cut face there may be systematic regional variations of stress near large intrapulmonary airways and blood vessels as well as the visceral pleura (23–31). In this thought experiment, the position and orientation of the cutting plane are arbitrary, and as such, the average state of stress everywhere within the lung must be precisely the pleural pressure. Moreover, that the pleural pressure is usually negative implies a state of tension in the tissues. The parenchymal tissue network transmits this tension from the pleura into the lung tissue.

We next consider this lung parenchyma tissue network at the level of microstructure (Figure 2). It is now well established that the parenchymal microstructure

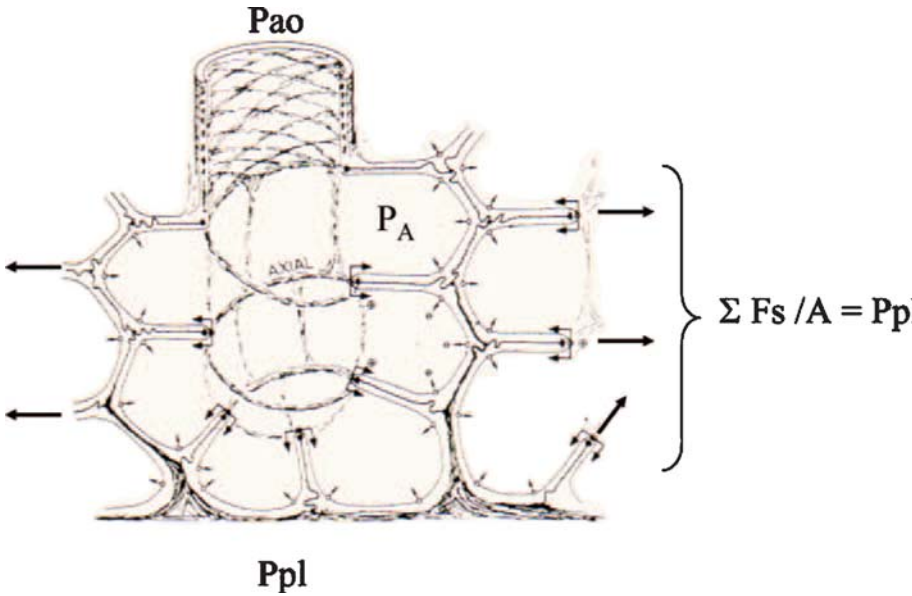

Figure 2 At the level of lung microstucture, alveolar geometry and elastic recoil are set by a balance of interfacial and tissue forces. In the absence of gas flow, gas pressures are everywhere equal, in which case we can set Pao $= P_A = 0$. Although distending stresses are concentrated in and transmitted by discrete alveolar septa, these concentrated septal forces (indicated by *arrows*) can be summed over a parenchymal region encompassing many alveoli and divided by the total cross-sectional area, yielding a distending stress. From Figure 1, this stress must be equal to Ppl. If the pressure on the inside of an airway or an alveolus is Pao and that on the outside is Ppl, then the transmural pressure for either structure is Pao-Ppl or simply P_L, the transpulmonary pressure. Adapted from Reference 13.

functions as a tension-supported lattice (10–14). As described below, the key distending stress—the transpulmonary pressure—is transmitted throughout parenchymal tissues and distends all intrapulmonary structures. This distending stress originates largely in the mechanics of the alveolar surface film and confers most of the parenchymal shear stiffness and the associated forces that are critical in maintaining the shape and function of the organ, including each vessel, airway, and alveolus. At each of these levels this distending stress is essential to lung function; it is a primary determinant of lung stability, the distributions of perfusion and ventilation, ventilation-perfusion matching, airway obstruction, and expiratory flow limitation (32–43).

The central importance of the surface film and the distending stress in these processes are not in dispute, and as described below, the roles of physical forces at the cellular and subcellular level are now becoming well established. But before moving to the cellular level, we ask, what are the stresses that act to distend an alveolus, intrapulmonary airway, or intrapulmonary blood vessel?

The Special Role of Transpulmonary Pressure

Although there are systematic departures, as described below (23–29), the effective stress acting on the outside of each of these structures is the same and approximately equal to the pleural pressure. As Ppl becomes more negative during the course of inspiration, the lung, the airway, the alveolus, and the vessel all experience an increase in distending stress. The effective stress acting on the inside of these structures is quite different, however. In the case of the blood vessel, the internal pressure is the local vascular pressure, Pv, and therefore the pressure difference distending the vessel wall, or the transmural pressure, is Pv–Ppl. During a normal lung inflation, pleural pressure becomes more negative, causing the lung to inflate, vascular transmural pressure to increase, and blood to accumulate in the thoracic cavity. Below we come to the issue of shear stresses acting on the endothelium owing to the flow of blood.

The transmural distending pressures of airways or alveoli are, respectively, Paw – Ppl and P_A – Ppl, where Paw is the local gas pressure in the airway and P_A the local gas pressure in the alveolus. If we limit attention to the case in which gas flow velocity is zero, such as at end-inspiration, end-expiration, or during a breath-hold, all gas in the lung will be at hydrostatic equilibrium and therefore the gas pressure will be everywhere equal and the same as the pressure at the airway opening, such that $P_A = Paw = Pao$. In that case, the transmural pressure distending an airway or an alveolus will become approximately Pao – Ppl, which we recognize immediately as the transpulmonary pressure. Thus, the transpulmonary pressure is the pressure difference that acts to distend not only the organ but also the alveolus and the airway.

An important departure from this simple description arises because intraparenchymal vessels and airways have mechanical properties different from those of the parenchymal tissues in which they are embedded. In the vicinity of

an airway or blood vessel, therefore, parenchymal distortions arise during the act of breathing, and the resulting stresses that act to distend these structures depart systematically from Ppl. This phenomenon is called elastic interdependence (10), and its effects on the distensibility of airways and vessels have been investigated extensively (23–29, 44–46).

STRESS INVARIANTS, LENGTH SCALES, AND TIMESCALES

Several characteristic scales for stress and time can be used to guide our thinking. Indeed, some of these seem to be invariants or regulated set points (Table 1).

Transpulmonary Pressure

At the macro level, the total lung capacity (TLC) in the adult human is achieved when P_L approaches 30 cm H_2O. Interestingly, 0–30 cm H_2O is the working range of transpulmonary pressures independent of lung size, body mass, or even lung development from neonate to adult (47–49). Even more remarkably, in species spanning a wide range of body masses, the working range of transpulmonary pressure is always the same, from 0 to 30 cm H_2O (50–52).

Interfacial and Tissue Elastic Stresses

Moving to a smaller length scale, we encounter the gas-liquid interface and interfacial forces. Most of the transpulmonary pressure is supported by alveolar surface tension; the balance is supported by lung tissue stresses (13, 30, 31, 53, 54). Although the surface tension can be higher during film expansion and approach zero during film compression, across all species the equilibrium surface tension in the alveolus is close to 25 dynes cm^{-1} (54). The law of Laplace states that the pressure difference acting across the gas-liquid interface is proportional to the surface tension and inversely proportional to the radius of curvature of the interface, and across species spanning three decades of body mass, M_b, from bat

TABLE 1 Characteristic levels of stress or force in lung structures

Equilibrium surface tension	25 dynes cm^{-1}
Transpulmonary pressure	0–30 cm H_2O (0–3000 Pa)
Shear stress at vessel wall	~1 Pa
Tensile stress in CSK	$\sim 10^2$–10^5 Pa
Stress in focal adhesion	~5000 Pa
Stress-generating capacity of contractile machinery	$\sim 10^5$ Pa
Forces generated by molecular motors	~1–10 pN

to dog, alveolar radius increases only weakly, with M_b, going as $M_b^{1/8}$ (9, 55). Therefore, if transpulmonary pressure and equilibrium surface tension are both invariant with body mass, then interfacial forces must play a relatively larger role in smaller species, and conversely (51).

Tissue Frictional Stresses and the Structural Damping Law

When they are deformed, lung tissues generate both elastic and frictional stresses. If tissue frictional stress is expressed as a tissue resistance, then lung resistance can be given as the sum of airway resistance and tissue resistance (56, 57), and at frequencies corresponding to quiet tidal breathing, lung tissue resistance typically exceeds airway resistance (58–60). This description is convenient and widely used, but to describe tissue friction as a flow resistance is to imply that there arises within lung tissues a stress analogous to that which results from the flow of a viscous fluid. The concept of a viscous stress as applied to lung tissue friction is now understood to be erroneous, however (61). Bayliss & Robertson (62) and Hildebrandt (63) demonstrated that frictional stress in lung tissue is dependent upon the amount of expansion but not the rate of expansion, findings that are fundamentally incompatible with the notion that friction is caused by a tissue viscous stress. If not in a viscous stress, how then does tissue friction arise, and how is it properly described?

With different lung tissue compositions and various physiological circumstances, tissue elastic and tissue frictional stresses vary greatly, but the relationship between them turns out to be very nearly invariant; the frictional stress in lung tissues is almost invariably between 0.1 and 0.2 times the elastic stress, where this fraction is called the structural damping coefficient (61). It is a simple phenomenological fact, therefore, that for each unit of peak elastic strain energy that is stored in lung tissue during a cyclic deformation, 10% to 20% of that elastic energy is taxed and lost irreversibly to friction. This fixed relationship holds at the level of the whole lung (60, 64), isolated lung parenchymal tissue strips (65), isolated smooth muscle strips (61, 66), and even isolated living cells (67–69). This close relationship between tissue frictional and elastic stresses is called the structural damping law (61, 63, 70, 71) or sometimes the constant phase model (64). The structural damping law implies that frictional energy loss and elastic energy storage are tightly coupled. As described below (see The Molecular Basis for Lung Mechanics, below), the sawtooth length-extension curve of some proteins offers a clue, but the precise molecular origin of this phenomenon remains unknown (72).

Endothelial Shear Stress and Murray's Law

The flow of blood in the pulmonary vascular tree exerts a shear stress upon the endothelial cell. The shear stress is proportional to the fluid viscosity and the shear rate, where the shear rate increases in rough proportion with blood velocity and in inverse proportion with vessel radius. At each bifurcation within a branching vascular network, the vessel radius tends to decrease slightly; this tendency might

thus seem to favor an increased shear stress, but because blood flow is divided into two daughter vessels, the flow velocity deceases as well and thus would seem to favor a decreased shear stress. As described by Murray in 1926 (73), as one proceeds along the vascular tree from larger to smaller vessels, which of these competing factors wins out and how wall shear stress varies with branching generation depend upon details of vessel geometry. Murray considered that issue as a question of biological design; he reasoned that increased vessel radius would favor decreased vascular resistance and thus reduced cardiac work required to pump blood, but increased vessel radius would also require more blood, more tissue mass, and associated metabolic energy costs for maintenance of these tissues. With those two energetic factors in mind, he then calculated the branching configuration that would minimize the rate of net energy utilization needed to support a given flow of blood. He showed that the rate of energy utilization is minimized when the cube of the parent vessel radius is equal to the sum of the cubes of the daughter radii. This result has come to be called Murray's law, and in his result Murray seems to have captured an integrative principle of biology, for not only the vascular tree but also water transport in plants seem to conform to Murray's law (74).

How could this state of affairs come about? It is easy to show that Murray's law implies that the shear stress at the walls of the daughter vessels is equal to that in the parent. The shear stress would be roughly invariant throughout the vascular tree, therefore, because the effects of decreasing radius are just offset by those of decreasing velocity. Although systematic departures have been noted, it is usually a good first approximation that the wall shear stress anywhere in the vascular tree is the nearly the same and assumes a value on the order of 10 dynes cm^{-2}. It is now well established that shear flow over endothelial cells modulates release and/or activation of many mediators, growth factors, cytokines, and nuclear transcription factors (75–77). The endothelium exhibits mechanosensation, therefore, capable of local regulation of a multitude of cellular functions including vascular remodeling. Later in this review we address mechanisms for mechanosensing.

Stresses in the Focal Adhesion Complex

On a still-smaller-length scale, another important stress invariant arises at the level of the focal adhesion (FA). Force transmission between the adherent cell and the extracellular matrix (ECM) is not distributed continuously across the cell membrane but rather is localized to the spot welds called focal adhesions (FAs). The focal adhesion complex is composed of integrins that are attached in the extracellular domain to the ECM and in the cytoplasmic domain to vinculin, talin, α-actinin, paxillin, tensin, and the microfilament terminus (78–80). The focal adhesion complex of an adherent cell may play a role analogous to the peg of a pup-tent; the external tensile distending stress is transmitted through the peg and confers stiffness and shape stability to the tent (Figure 3). Similarly, the adherent cell may be dependent upon external distending stresses to maintain its shape stability (81–84).

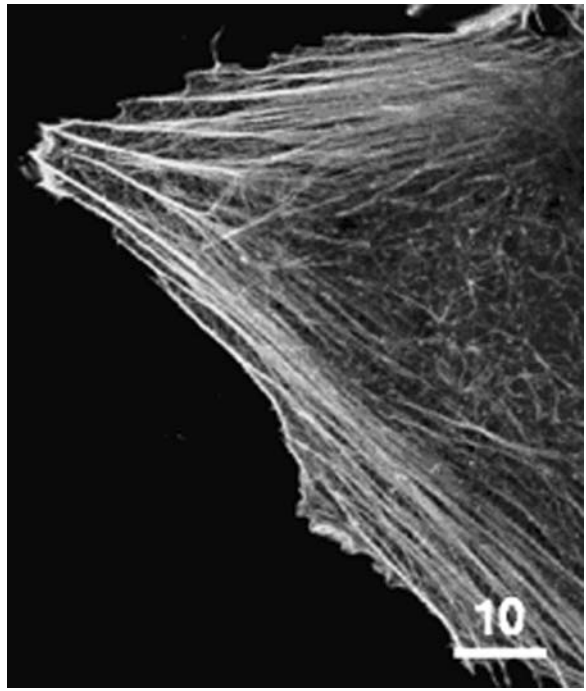

Figure 3 The CSK of the adherent cell appears to be under tension, with tensile stresses supported at the cell boundary by focal adhesions. If deformed, does the cell generate restoring forces mostly by resistance to elongation of line elements, or by reorienting them? Rat fibroblast is stained by antiactin antibody; scale bar = 10 μm.

Cell stiffness or contractile forces must be considered in the context of the ECM in which they reside. In this connection, there are marked differences between cells grown on two-dimensional (2D) versus three-dimensional (3D) substrates (85, 86). When grown on a flat 2D surface, cells initially attach to matrix molecules (e.g., collagen, fibronectin) laid down on the substrate but over time develop a matrix of their own that more closely mimics their in vivo environment. During this process, cells first adhere to the substrate through focal complexes that contain a relatively small number of FA proteins [vinculin, paxillin, focal adhesion kinase (FAK)] and that are roughly 1 μm in size (87, 88). Focal complexes grow into FAs, which serve as a point of attachment between the ECM and the cellular CSK, typically using the $\alpha_v\beta_3$ integrin. These, in turn, evolve into fibrillar adhesions that exert a tension on the matrix laid down by the cell, giving rise to extracellular remodeling through the exposure of cryptic binding sites in fibronectin, causing it to bundle and strengthen. Given ample time, the substrate takes on the nature of a 3D matrix, at which point the adhesions come to resemble those found in vivo, with a long, thin morphology in which paxillin, fibronectin, and α_5 integrin are

colocalized (85). This takes time, however—typically days—even in a dense cell culture (85). By comparison, cells grown either on or inside a 3D matrix in which the fibrous architecture—filament size, density, matrix compliance—from the onset resembles the cell environment in vivo immediately form 3D adhesions. Most prominently, these differences are reflected by cells that adhere more strongly to and migrate more rapidly through 3D matrices than to/on 2D substrates and that take on a different, more elongated morphology. Some of these differences are likely attributable to differences in integrin-mediated signaling. For example, autophosphorylation of FAK is downregulated in 3D relative to 2D systems, whereas phosphorylation of two other FA proteins, paxillin and mitogen-activated protein kinase (MAPK), is unaffected (85). Throughout this maturation process, various integrins are used, each with its own unique signaling characteristics, and both a compliant substrate and the $\alpha_5\beta_1$ integrin appear to be critical for the formation of typical 3D adhesions (85, 86).

Contractile Machinery and Cytoskeleton

Airways and blood vessels in the lung are each surrounded by a sheath of smooth muscle (89–91). To within an order of magnitude, virtually all muscles, whether striated or smooth, have the same intrinsic maximal stress-generating capacity, which is on the order of 10^5 Pa (9). The individual myosin motor generates forces that are in the pN range.

Virtually all cells attached to a substrate tend to contract. Although this is an obvious function of skeletal, cardiac, or smooth muscle cells, the role of contraction in nonmuscle cells is less clear. Contractility is, however, an important element in cell migration and therefore in the inflammatory response, wound healing, and metastatic disease. It may also play a fundamental role in maintaining cell adhesions in a state of tension, which may be important for signaling via receptors such as integrins, and is also an important determinant of cytoskeletal tension, as discussed further below.

Much of what we know about the forces that cells exert on the surrounding matrix comes from measurements by a method known as traction microscopy. Dembo & Wang (92) were the first to show that the spatial distribution of these tractions can be mapped from measurements of the displacement field created in a flexible substrate on which the cell is adherent. Measurement of the displacement field is accomplished by tracking small beads, typically 0.2 μm in diameter, embedded near the surface of the substrate gel. To mitigate the extreme computational requirements associated with the method of Dembo & Wang, Butler et al. (93) developed Fourier Transform Traction Microscopy (FTTM) (Figure 4). Although there remains some controversy concerning competing computational approaches (94), FTTM is equally rigorous and has become widely used (84, 95–97). In an alternative approach, elastomer microposts and micropatterned elastic substrates have been used to measure cell tractions (87, 98). It is important to recognize, however, that all three approaches are performed with the cells spread on a flat surface.

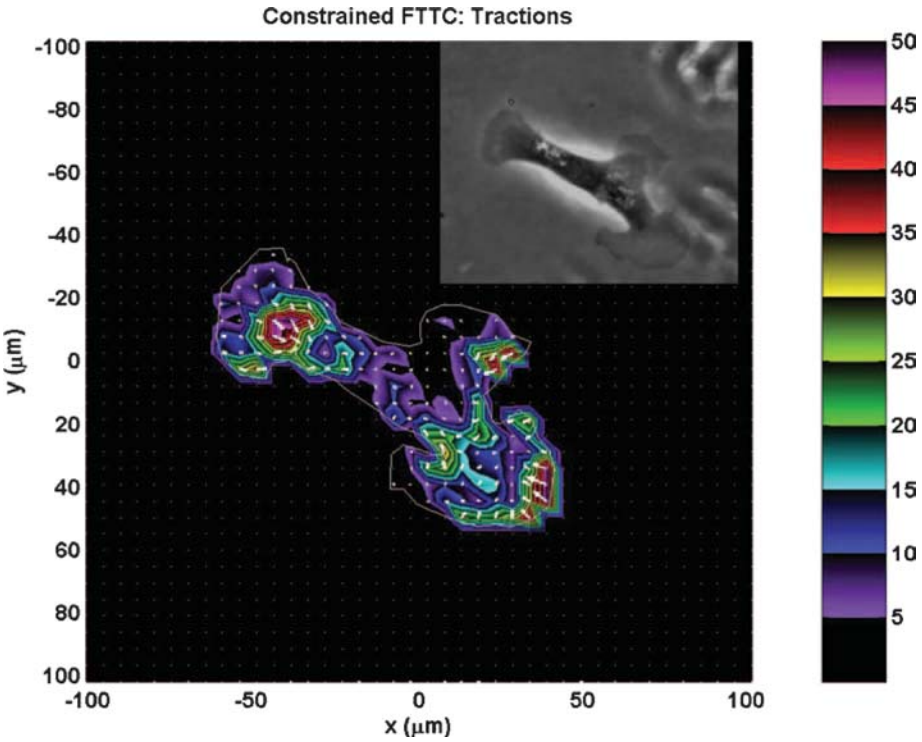

Figure 4 Traction microscopy creates an image of the physical stresses (tractions) applied by an endothelial cell to its substrate, shown here from a study of responses to hypoxia via p38 MAPK and Rho kinase–dependent pathways. Colors show the magnitude of the tractions in Pa; see color scale. Arrows show the directions and relative magnitudes of the tractions. From Reference 97.

Measurements have been made on a variety of cell types, but most often contractile cells are used, including fibroblasts, myocytes (87), or smooth muscle cells (96). In general, cells exert tractions on the substrate that are consistent with intracellular contraction, that tend to be concentrated at FAs, and that tend to be greatest near the outer perimeter of the cell. Total contractile forces have been measured in the range of ∼20 nN in fibroblasts but as high as ∼70 nN in contracting myocytes (87). Interestingly, the stress acting at individual FAs is found to be relatively constant, in the range of approximately 5.5 kPa (55 cm H_2O), and similar for both cell types (87). This value appears to be invariant, so that as the contractile force exerted by the cell varies, so does the contact area of the FAs and, presumably, the number of integrin receptors involved. The mechanism remains unclear but may include local recruitment of filamin, actin, and talin 1 (99, 100).

Perhaps of greater relevance to the lung, Stamenovic and coworkers (84, 96) measured the contractile stresses generated within airway smooth muscle cells

cultured on a 2D surface and found values ranging up to approximately 2 kPa. Note that this is the computed mean stress acting over the cross section of the cell normal to its primary axis of contraction and is not directly comparable to the values for FA stress given above. Other measures in more realistic external environments or with isolated muscle fibers demonstrate that contractile stress is almost invariant, having a value on the order of 10^5 Pa in all contractile tissues (9). Differences between this value and the one for smooth muscle cells grown in culture may be attributable to two facts: (*a*) The CSK in cultured cells is organized more for adhesion than contraction (Figure 3), and (*b*) in 2D culture the level of expression of contractile proteins is reduced (101).

Elastic Similarity

McMahon (9) has suggested a unifying principle of biological design with far-reaching implications and remarkable explanatory power. This principle, called elastic similarity, holds that across species spanning a wide range of body mass, M_b, the bones and muscles are designed so as to bend by approximately the same amount. Although deceptively simple, from elastic similarity it follows more or less directly that energy metabolism scales as $M_b^{3/4}$, respiratory frequency and heart rate as $M_b^{-1/4}$, lung volume and tidal volume as M_b^{1}, alveolar radius as $M_b^{1/8}$, transpulmonary pressure and arterial pressure as M_b^{0}, airway resistance as $M_b^{-3/4}$, lung and chest wall compliance as M_b^{1}, mechanical time constants as $M_b^{1/4}$, and clearance rates and reaction rates as $M_b^{1/4}$; in each instance the indicated relationship falls close to observations. McMahon has pointed out that if time constants go as $M_b^{1/4}$, respiratory frequency goes as $M_b^{-1/4}$, and lung recoil goes as M_b^{0}, this guarantees that lungs of all sizes are given the same number of time constants to empty during a passive expiration. The questions of how bending might be sensed at cellular and molecular levels, and how mechano-sensing cues might trigger remodeling, are addressed below.

CYTOSKELETAL STRUCTURE, STIFFNESS, AND STRESS TRANSMISSION

Although the lung parenchyma (Figure 2) and the CSK (Figure 3) are superficially distinct in structure and widely disparate in scale, they share a deep similarity in the mechanism that confers stability of shape. Ordinary solid materials retain a defined shape in the absence of a distending stress, but not so for pressure-supported structures such as the lung, which would collapse, or the adherent cell, which would round up. Shape stability of both the lung and the adherent cell is determined mainly by their respective distending stresses.

Understanding of the distending stress as the main source of shape stability began approximately 30 years ago, when one of the major conceptual problems in respiratory mechanics was parenchyma resistance to distortion of shape. This

problem is of great physiological and pathophsyiological importance because, besides the transpulmonary pressure itself, it is the resistance of the lung parenchyma to shear distortion that is the preeminent factor acting to maintain the patency of intrapulmonary airways, intrapulmonary blood vessels, and individual alveoli. Each of these structures has a natural tendency to collapse, but shear distortion of the surrounding parenchyma creates restoring stresses that act to oppose that collapse (10–14, 102). Importantly, this elastic interdependence creates restoring stresses that are proportional to P_L and comparable in magnitude. The question was, why?

Shape Stability of Stress-Supported Structures

The measure of resistance to shape distortion of a material is the shear modulus (shear stiffness), but early predictions of the shear modulus for lung parenchyma far exceeded observed values (3, 103, 104); given the amounts of its constituents and their material properties, the lung seemed to be far floppier than it reasonably ought to have been. Perhaps more importantly, these initial theories also failed to explain the central organizing feature of lung tissue mechanical behavior, namely that its shear stiffness increases in direct proportion to inflating pressure; the shear modulus of the lung is simply 0.7 P_L (14). On a much smaller scale, an entirely parallel relationship was subsequently shown to hold between the shear stiffness of the CSK and its distending stress (82–84, 96, 105–109).

Kimmell, Kamm, & Shapiro (11) first identified, and Kimmel & Budiansky (12, 110) and Stamenovic (3) later elaborated upon and generalized, the physical basis of such behavior. As applied either to the lung parenchyma or to the CSK, earlier theories had made the traditional assumption that as one proceeds to smaller and smaller scales, the microscale strain of structural members faithfully follows the local macroscale strain of the matrix or network; this condition is called affine deformation. The approach introduced by Kimmel et al. relaxed that assumption and instead considered the discrete nature of stress-bearing members at the microscale and the nature of their connectedness. It is the limited nature of this connectedness that turned out to be the radical feature. Kimmel and coworkers showed that depending on that connectedness, the structural matrix composed of discrete stress-bearing members resists shape distortion not so much by resistance to elongation in those microstructural members, as it must in an affine continuum, but more so by reorientation of those members. When placed under load, the structural elements move relative to one another in a nonaffine manner, changing their orientation and spacing until a new equilibrium configuration is attained. Importantly, the bigger the initial tension carried by those elements, i.e., the bigger the prestress[2] (the inflating pressure in the case of the lung and tractions in the case of the adherent cell, as described below), the smaller the deformation that the structure

[2]The terms prestress and distending stress are often used interchangeably. Prestress, in particular, refers to the value of the distending stress before the system is deformed incrementally or before the distending stress is varied incrementally.

must undergo before attaining a new equilibrium configuration. As the prestress increases, therefore, the resistance to a change of shape increases in proportion. Indeed, in such structures the macroscopic shear stiffness can remain finite and small even as the stiffness of microstructural members becomes infinitely large.

This line of thinking explained why the material shear stiffness of lung parenchyma is much smaller than earlier theories had predicted and at the same time revealed why the shear stiffness must increase in direct proportion to the distending stress. The same physics applies at the level of the CSK, where this idea subsumed the controversial tensegrity hypothesis of cell mechanics (111–113), generalized it, and put it on firm theoretical and experimental footing (82–84, 96, 105, 106, 108, 114–117).

A complementary perspective to CSK mechanics derives from the mechanics of polymer solutions or gels (118–122). Each filament in the matrix is treated as a semiflexible biopolymer and is characterized by its bending stiffness as influenced by thermal fluctuations. As with the earlier models, when no initial stress is imposed, as that by external tractions, the theory cannot account for the observed stiffness of the CSK. When an initial stress or strain is imposed, however, these gels progressively stiffen as the fluctuations in individual filaments are pulled out and the polymer chains lose configurational entropy. In both the tensegrity and biopolymer theories, two features are critical: the finite initial prestress imposed by the combined effects of internal contraction and external tethering, and the nonaffine nature of the deformations at the microscale.

Once one understands behavior at the microscale and derives values for macroscopic parameters such as the shear modulus, a continuum approach can once again be adopted to analyze cellular stress and deformation, but all information about strain in individual microstructural elements is then lost (82, 84, 106, 120, 123).

Stress Transmission Pathways Within the Cytoskeleton

What is the pathway of stress transmission within the CSK? To address this question, Hu et al. (124) developed intracellular stress tomography. They coupled a ferromagnetic microbead bound tightly to the CSK via integrins and FA plaques (Figure 5, *pink arrow*). Next they applied a sinusoidal magnetic field, causing a cyclic mechanical torque on the bead and resulting oscillatory distortions of the CSK (in the range of 5–300 nm). They then created images of the synchronous displacements of specific cytoskeletal structures. If elastic moduli of the CSK were homogeneous and isotropic, then the corresponding map of displacement gradients would represent intracellular stress. However, because that assumption is unlikely to be accurate, these maps can only be thought of as a rough approximation to the intracellular stress distribution, although they are no less interesting. If anything, they probably underestimate the degree of stress heterogeneity because the CSK is likely to be both denser and have a higher concentration of stress fibers in the vicinity of FAs. These maps show that in the living adherent cell, the distribution of mechanical strain is punctate and transmitted over long distances through the cytoplasm. They also show convergence of strain fields at the intracellular domain of the FA plaque.

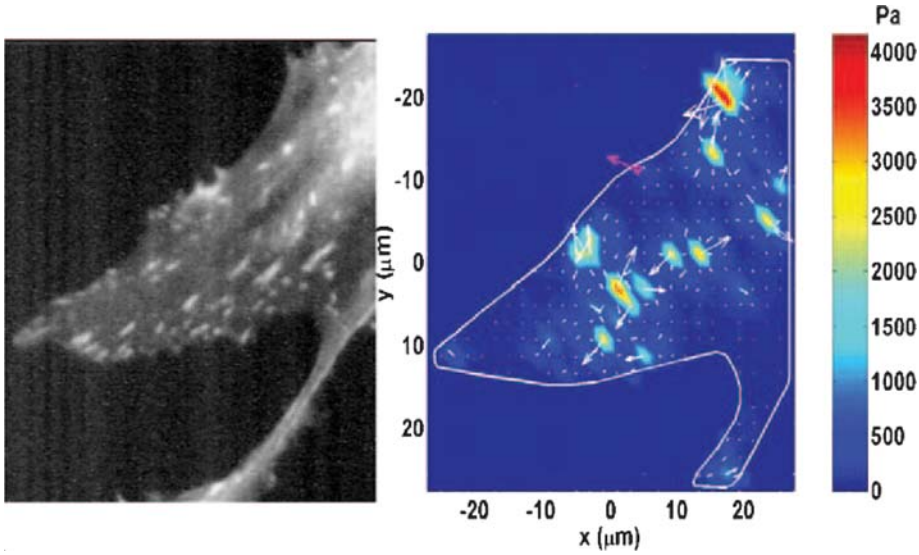

Figure 5 Intracellular stress tomography. (*Left*) Fluorescently labeled paxillin in focal contacts imaged 1 μm above the cell base. (*Right*) Stresses induced in those structures by the cyclic torque of a bead on the cell apex (*pink arrow*). From Reference 124.

Stress Transmission To and Through the Nucleus

Maniotis et al. (125) showed that when integrins are pulled by micromanipulating bound microbeads, cytoskeletal filaments transmit stresses to the cell nucleus and cause nucleoli redistribution. Using the stress tomography method described above, Hu et al. (126) mapped the displacements of the nucleolus, an intranuclear organelle crucial for ribosomal RNA synthesis. Using micropipette aspiration and atomic force microscopy indentation of isolated nuclei, Dahl et al. (127) showed that rheology of the nucleus exhibits power law rheology and implies an infinite spectrum of timescales for structural reorganization; they speculated that this behavior may have fundamental implications for regulating genome expression kinetics. As described below, power law behaviors seem to be a pervasive feature of cytoskeletal dynamics.

SCALE-FREE BEHAVIOR, CYTOSKELETON REMODELING, AND GLASSY DYNAMICS

Recently there has been established a striking analogy in which the CSK of the adherent cell is seen to adjust its mechanical properties and modulate its malleability in much the same way that a glassblower fashions a work of glass (67, 68, 128, 129). However, instead of changing temperature, the cell changes a temperature-like property that has much the same effect.

Fabry et al. (67, 68) first suggested that the CSK may behave as a glassy material. They measured stiffness and friction in a variety of cell types in culture, including the human airway smooth muscle cell. Fabry et al.'s reports contained two surprising results. First, they had set out to identify distinct internal timescales (i.e., molecular relaxation times or time constants) that might reflect molecular dynamics of proteins integrated within the CSK lattice, and in particular they had expected to find relaxation timescales corresponding to myosin-actin cycling rates. Surprisingly, over a spectrum spanning five decades of frequency, f, and in all five of the cell types investigated, they found no characteristic timescales. Rather, stiffness increased as f^{x-1}, implying that relaxation times were distributed as a power law, with a great many relaxation processes contributing when the frequency of the imposed deformation was small but fewer as the frequency was increased and slower processes became progressively frozen out of the response. Thus, no distinct internal timescale could typify protein-protein interactions; all timescales were present simultaneously but distributed very broadly. Because no distinct timescales characterize the response, behavior of this kind is called scale-free. Using other techniques and differing cell types, others have confirmed that CSK dynamics are scale-free (130–134).

Fabry et al.'s second surprise was the discovery of an unexpected relationship among changes in cell mechanics that arise when CSK constituents are modulated. In the living cell, rheology of the CSK matrix is influenced by many structural proteins and their interactions. Despite this complexity, if stiffness or friction data are appropriately scaled and then plotted versus x (which is readily determined from the power law exponent of stiffness versus frequency), all data collapse onto the very same relationship (Figure 6) regardless of the cell type studied, the signal transduction pathway activated, or the particular molecule manipulated (67, 135).

Purely as a matter of phenomenology, the observations described above firmly establish that the parameter x determines where the CSK sits along a continuous spectrum of solid-like versus fluid-like states (68); in the limit that x approaches 1, the behavior approaches that of a Hookean elastic solid, and in the limit that x approaches 2, the behavior approaches that of a Newtonian viscous fluid. Values of x for adherent living cells fall in the range of 1.1 to 1.3, placing them closer to the solid than the fluid state (Figure 6). Moreover, the parameter x was subsequently found to bring together into one phenomenological picture not only cytoskeletal stiffness and friction but also remodeling (128, 129). Moreover, there is a direct relationship between the effective temperature x and the structural damping coefficient η; $\eta = \tan((x\text{-}1)\pi/2)$, and when x is close to 1, x is approximately $1 + \eta$.

With regard to mechanism, classical theories of viscoelasticity and equilibrium systems fail to account for these observations (128), and the physical significance of the parameter x remains elusive. The working hypothesis holds that the CSK behaves as glassy system and that the parameter x, which is easily measured, corresponds to the effective temperature of the CSK lattice (67, 128, 129,

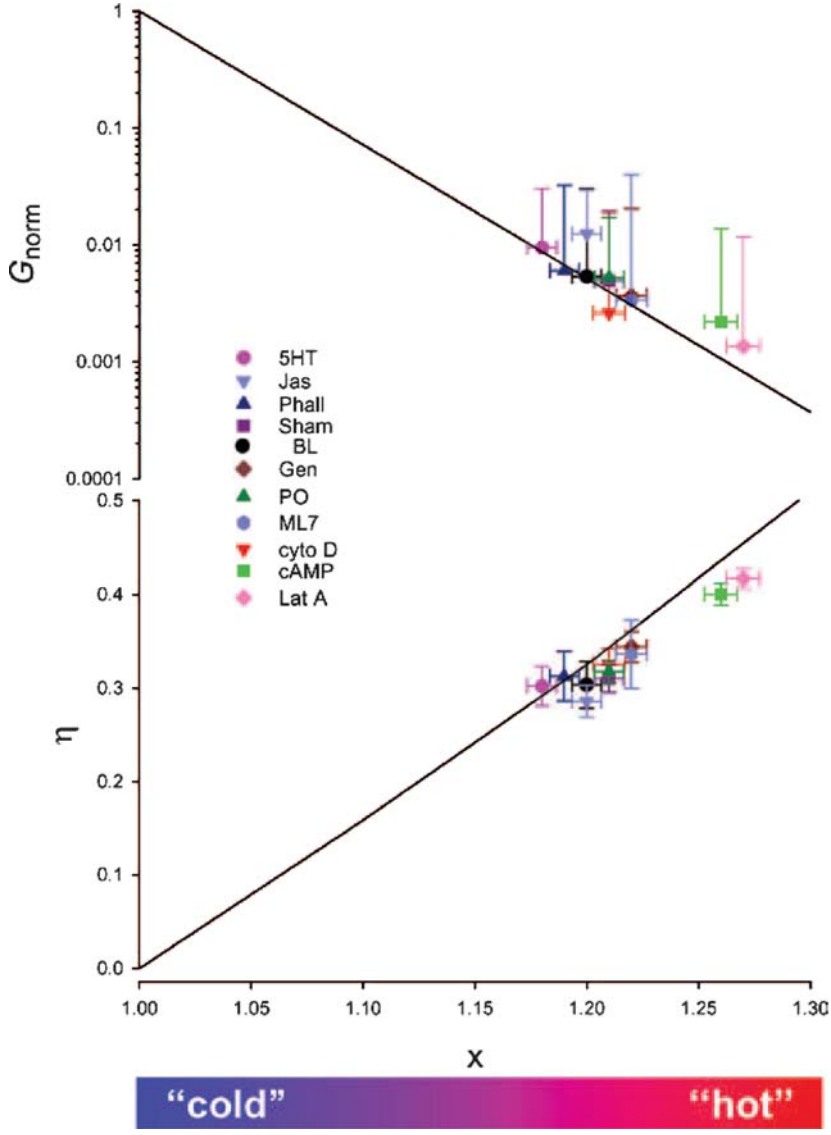

Figure 6 The CSK sits along a continuous spectrum of solid-like versus fluid-like states, where the limit $x = 1$ corresponds to a perfect Hookean elastic solid and the limit $x = 2$ corresponds to a perfect Newtonian viscous fluid. Master curves: (*upper panel*) normalized stiffness $G_{\text{norm}} = g'$ (0.75 Hz)/g_0 and (*lower panel*) hysteresivity η (0.75 Hz) versus x. The solid lines are as predicted from the equations below: $\ln G_{\text{norm}} = (x-1)\ln(\omega/\omega_0)$ (*upper panel*), $\eta = \tan((x-1)\pi/2)$ (*lower panel*). g_0 and f_0 are determined. Symbols denote baseline, latrunculin A, cytochalasin D, phallacidin, phalloidin oleate, jasplakinolide, genistein, 5-HT, db cAMP, and ML-7. Adapted from Reference 193.

135–137). In that case the system is regarded as being frozen when x is close to 1 and melted when x is close to 2. Although the underlying physics remains poorly understood, strong experimental support for x as an effective temperature of the cytoskeletal lattice has recently been reported (128, 129). In a recent publication, this analogy has been supported by a broader range of biophysical observations (128, 129).

To explain these findings, Bursac et al. (128) have suggested the following physical picture. They imagine trapping of a CSK structural protein or protein complex in a deep energy well, i.e., a well so deep that thermal collisions are insufficient to drive it out of the well (67, 68, 128, 129, 135, 138). If thermal forces are insufficient, then hopping out of the well is imagined to be driven by nonthermal energies that are much larger than k_BT (where k_B is Boltzmann's constant and T is thermodynamic temperature) but can be expressed nonetheless as an "effective temperature" of the CSK matrix. Formally, the term "temperature" means molecular motion; temperature carries with it the connotation of molecular collisions and resulting agitation caused by ongoing molecular bombardments of thermal origin. Here the term "effective temperature" is meant to carry with it a similar connotation of molecular agitation caused, however, by processes that may be of nonthermal origin. A protein conformational change fueled by ATP hydrolysis, for example, releases energy that is greater than thermal energy by 25-fold (139) and does so at the rate of more than 10^4 events per second per cubic micron of cytoplasm (138). Accordingly, such events would have the potential to jostle a neighboring structure rather substantially and dislodge it from a relatively deep energy well.

Physical interactions that lead to trapping may include molecular crowding, hydrogen bonding, or weak cross-linking (140–144). With regard to molecular crowding, the volume fraction of macromolecules within the cell approaches the maximum packing fraction that is possible; the mean distance between macromolecules is only 2 nm (145). The molecular space within a cell is so crowded, in fact, that crowding can change binding affinities between specific proteins by orders of magnitude (142, 144, 146, 147). If trapping is due to nonspecific mechanisms such as molecular crowding or hydrophobic interactions, then the specific properties of cross-linking molecules may be of only secondary importance. But if trapping has its origins in cross-linking of CSK filaments, then the density and the specific type of cross-links and CSK filaments, as well as the dynamics of their specific interactions, may be crucial (120). Many of the cytoskeletal modulations used to date alter both macromolecular packing and the dynamics of cross-linked filament networks (148), and thus they cannot determine which of the two interactions may play a dominant role. Regardless of the particular interaction, trapping is hypothesized to arise owing to the insufficiency of thermal energy to drive CSK structural rearrangements (140). The collapse of data onto master curves (Figure 6) suggests that specific molecular interactions influence CSK stiffness and friction, but only to the extent that these interactions can modify the effective temperature.

Is the Effective Temperature Set by the Distending Stress?

Recently reported data from mechanical measurements of cultured cells show that stiffness of the cytoskeletal matrix is determined by the extent of distending stress borne by the CSK, where distending stress can be changed either by modulating the contractile state of the cell or by mechanical stretch (82–84, 96, 105, 106, 108, 114–117, 149). At the same time, rheological measurements show that cytoskeletal stiffness changes with frequency of imposed mechanical loading according to a power law (150). Stamenovic et al. (150) and Trepat et al. (149) examined the possibility that these two empirical observations might be interrelated. Their findings revealed that the transition between solid-like and liquid-like states of the CSK, and the effective temperature that describes that transition, seemed to be controlled by cytoskeletal distending stress. They took this result to imply that the depth of the energy wells described above must increase as cytoskeletal tension increases. A similar behavior was subsequently reported in tensed cross-linked actin gels (120), and an alternate explanation derived from the theory of semiflexible biopolymers has been proposed (123).

SENSATION OF FORCE: MECHANOSENSING

That cells sense and respond to externally applied or internally generated stresses is now widely recognized as an essential feature of cell function. Endothelial cells, for example, respond to hemodynamic shear stresses as low as 1 Pa through activation of Src, FAK, and MAPKs. Signals are often mediated by the $\alpha_v\beta_3$ and $\alpha_5\beta_1$ integrins (151) and involve the small Rho GTPases. Consequences of stimulation are many and varied but include intracellular reorganization, changes in protein expression, and the regulation of proteins involved in extracellular remodeling. Many of these same effects can be observed in endothelial cells subjected to mechanical strain, so the response to stress may be relatively independent of the manner in which force is applied.

Candidates for the transducer that converts mechanical force into a biochemical signal include mechosensitive ion channels whose conductivity changes in response to stresses in the cell membrane (152, 153), as well as other force-induced changes in protein conformation that may alter either binding affinity or kinase activity of proteins subjected to force. Mechanosensitive ion channels presumably change their conductance either as a result of stresses within the cell membrane or as a consequence of forces transmitted directly to the channel protein(s) via membrane-associated proteins. An example of the latter is found in hair cells of the inner ear, in which forces are transmitted from the tip of one stereocilium to a channel on the side of a neighboring one via a thin connecting filament, the tip link. As the collection of stereocilia is displaced by vibrations in the cochlear fluid, forces in the tip link are transmitted to the channel, causing it to change its conductance. In other mechanosensitive channels, such as the mechanosensitive

channel of large conductance, it is thought that membrane tension itself directly mediates channel opening. Support for this mechanism comes from molecular dynamic simulation, although the simulated changes in pore dimension still appear insufficient to explain the entire process of channel activation (154, 155).

In the lung, current evidence points to a role for ion pumps in the activation of alveolar epithelial cells by stretch (153). Through the use of epithelial cells grown on a flexible substrate to simulate the cyclic stretch that these cells experience during normal or assisted breathing, Na^+ pump activity was found to increase in proportion to the magnitude of stretching (153). This may be a beneficial response to increases in epithelial layer permeability associated with damage to the alveolar wall from overdistention (156, 157). Interestingly, cells cultured for five days, sufficient time to lay down a matrix of their own, responded only when the levels of substrate stretch were very high, corresponding to an approximately 37% increase in surface area (153). Although these levels of strain may seem high, direct measurement of changes in epithelial basement membrane area can be as high as 40% (corresponding to a linear strain of 18%) when lung volume increases from 24% TLC to 100% TLC (158). Cells subjected to noncyclic, steady stretch showed no increase in pump activity, suggesting that the cells can accommodate to static changes in area, but not to cyclic ones.

Other studies have examined the role of increased production of reactive oxygen species in ventilator-induced lung injury (159), which in turn can lead to increased production of inflammatory cytokines (160) and increased neutrophil sequestration (161). Again, cyclic stretch, this time a 15–30% biaxial strain (32–69% increase in surface area) was used, and such large strains may contribute to either cell detachment or loss of cell viability. Although the underlying mechanism causing the change in the production of reactive oxygen species remains unclear, it may involve the possible role of changes in mitochondrial shape or size (159), as may occur in endothelial cells (162, 163).

Much of the stress-induced signaling originates in FAs, and these are also the sites at which forces tend to be focused (77, 124). Thus, many have speculated that FAs represent also the location of mechanosensation, the biological process that transduces a mechanical force into a biochemical signal. It is hardly surprising that some of the same conformational changes that occur as a result of ligand-receptor binding, for example, may be brought about by forces transmitted by these same proteins, especially those in the FA complex. That such conformational changes typically lead to nanometer-scale domain movements under forces on the order of 10 pN lends indirect support for this concept. Corresponding energies for such deformations are then in the range of 10 pN·nm, or a few multiples of the thermal energy, k_BT—large enough to avoid frequent, unintended thermal activation but low enough so that levels of force typical of those transmitted through an FA are sufficient to cause activation. Compare this to estimates that each integrin in a mature FA under normal cell tension experiences a force of at least 1 pN (87), given the assumption that the integrins are close-packed. In separate experiments, it has been demonstrated that forces as small as 2 pN can break bonds in an initial

contact (164), thought to be a bond between talin-1 and actin filaments, whereas subsequent strengthening under force, presumably by the recruitment of vinculin, can increase bond strengths to more than 60 pN. Proteins such as titin unfold or denature with forces in the range of tens to several hunded pN, depending on the rate of increase in force, and many important molecular bonds (e.g., biotin-streptavidin) rupture at forces in the range of 100 pN (reviewed in Reference 165). Therefore, the range of force between 1–100 pN and energies of 10–100 pN·nm are likely crucial in the control of cellular processes by mechanical force.

Experimental evidence for the role of conformational change in mechanosensing is gradually accumulating. In one set of experiments, Sawada & Sheetz (166) grew cells on a flexible substrate and then incubated them in a detergent to remove the cell membranes and thereby eliminate any potential influence of membrane ion channels. Then, comparing the proteins that bound to these exposed CSKs with the substrate stretched or relaxed, they found significant differences, notably that FAK, paxillin, and p130Cas (166) preferentially bound to the stretched substrate. In a separate set of experiments, Src activation was imaged directly and locally as force was applied to a cell through a tethered bead with an optical trap (167). The response was immediate and generally localized to the FAs experiencing force. Interestingly, the researchers observed a wave of Src activation emanating from the site of force application, propagating at a speed of approximately 18 nm s^{-1}. Although these experiments are not capable of identifying the mechanism that initiates the signal, they do demonstrate that the signaling is immediate, is initiated in the regions of high force, and can be propagated to other regions within the cell.

More direct experimental and computational evidence, through the use of molecular dynamics, demonstrates that force application can expose cryptic binding sites, for example in fibronectin (168), leading to bundling of this ECM protein. Similar cryptic binding sites have been identified in several intracellular proteins—vinculin (169), α-actinin (170), and potentially talin (171, 172)—all present in a FA. Although not compelling, this at least suggests that similar phenomena may occur intracellularly, leading either to mechanical reinforcement or the initiation of a signaling cascade.

Cytoskeletal changes can also occur rapidly and may be locally mediated. Experiments on human neutrophils subjected to elongation in narrow channels comparable in size to the pulmonary capillaries exhibit a rapid (within seconds) and significant (by a factor of two) reduction in shear modulus (173). This drop in modulus can be reversed on a timescale of less than one minute. Such deformations give rise to numerous changes, such as increased calcium ion concentration and increased expression of two adhesion receptors, CD18 and CD11b (174), but the change in modulus appears to be linked to a transient reduction in polymerized actin (175). These experiments highlight the dynamic nature of force-induced changes in cell structure and also point to the limitations of assuming that the cell can be treated, even on relatively short timescales, as an inert material with constant properties.

Changes in protein conformation or modulation of channel conductivity are not the only mechanisms by which a cell transduces stress. Recent studies demonstrate that as the transepithelial pressure rises—as during airway constriction, when epithelial folds push the opposing epithelial surfaces against one another—the resulting stresses cause the spaces between neighboring cells to shrink, squeezing out some of the intracellular fluid and bringing the lateral cell membranes into closer proximity. One consequence of this reduction in the lateral intercellular space is that the concentration of ligands shed from the lateral membrane, specifically heparin-binding epidermal growth factor, increases owing to the diminished width of the pathway for diffusion out of the lateral intercellular space, leading to enhanced activation of the EGF receptor (176). This then initiates a signaling cascade characterized by increased phosphorylation of the MAPK ERK1/2 within 15 minutes, and longer-term upregulation of early growth response-1 and transforming growth factor-β (177). These upregulated proteins also stimulate fibroblasts in close proximity to increase their collagen production (178), contributing to airway wall remodeling, one of the hallmarks of asthma.

Remodeling also occurs in the pulmonary vasculature. Vascular endothelial cells respond to stress in two stages. In the early stage, elevated shear stress due to increased blood flow, potentially in combination with other factors such as hypoxia, is thought to initiate a process that leads to vasoconstriction and possibly proliferation of vascular wall cells (179). This consequently leads to elevated resistance to blood flow and increased pulmonary arterial pressure, initiating the second stage. Increased hoop stress associated with higher arterial pressure (*a*) stimulates the endothelium to initiate a process that leads to increased levels of collagen synthesis (180) and (*b*) influences release, from the endothelium, of factors that ultimately produce smooth muscle hypertrophy and adventitial thickening. These processes cause the observed arterial wall remodeling (181). Thus, the process of arterial wall remodeling appears to be influenced strongly by the forces experienced by the pulmonary arteries, an effect that is predominantly mediated by the arterial endothelium.

THE MOLECULAR BASIS FOR LUNG MECHANICS

Whether we consider the extracellular matrix, whose structural integrity is primarily conferred by the collagen and elastin fibers, or the matrix of resident cells, whose stiffness is derived from the CSK of actin microfilaments, intermediate filaments, and microtubules, a full understanding of mechanical stiffness requires a look at the individual molecular constituents. In addition, as we discuss above, most of the fundamental mechanisms by which cells sense and respond to mechanical stimulus occur at the level of single molecules, such as those that comprise the FA complex.

In principle, all macroscopic elastic and frictional properties of cells or tissues can be derived from knowledge of single-molecule mechanics and the manner in

which the constituent molecules assemble into a 3D matrix. In practice, we are far from achieving that goal but have begun to take some important steps. Here we use, as an example, the microfilament matrix of the CSK to show how, once we attain a molecularly based appreciation of the structures, we can use this foundation to expand our understanding of critical mechanical properties.

Two evolving technologies form the basis for this approach: molecular dynamics simulation and experimental measurements on single molecules. Nearly a decade ago, the first measurements of the elasticity of a single protein were made using an atomic force microscope (AFM) tip (182) or a bead in an optical trap (183) functionalized so that it bound to the molecule of interest. One of the earliest proteins studied was titin, which was thought to be responsible for much of the elastic character of passive or relaxed skeletal and cardiac muscle. Through these initial and subsequent investigations, investigators revealed that titin consists of three elastic regions called the PEVK (rich in proline, glutamate, valine, lysine) domains, fibronectin type III domains, and the immunoglobulin (Ig)-like β-barrel domains. The first two of these behave as entropic springs (their resistance to stretch is due to a loss of configurational entropy), and the third, which is initially entropic in nature, exhibits a sawtooth pattern of force plotted against extension if stretched excessively (Figure 7*A*) (182). Each peak in the sawtooth pattern corresponds to the point at which one of the Ig domains reaches its limit, at approximately 250 pN with a pulling rate of 1 $\mu m\, s^{-1}$, and unfolds to an extended configuration, as depicted for a fibronectin domain in Figure 7*B* (194). In this manner, and owing to the stochastic nature of domain unfolding, a collection of titin (or fibronectin) molecules arranged in parallel, as in a sarcomere of skeletal muscle, would exhibit a constant force resisting pulling, while lengthening many times the initial length of the individual folded domains. As it turns out, domain unfolding is not thought to occur frequently in muscle under normal physiological conditions (185), but the same behavior has been discovered in several other structural proteins, notably spectrin (186), known for its role in the cortex of a red blood cell, and filamin A (187), one of the primary actin cross-linking agents in the CSK. Molecular dynamics simulations of a single Ig domain subsequently revealed the rich detail of behavior that occurs during unfolding and refolding as well as subtle differences between variations of the domain (188). One drawback of steered molecular dynamics (SMD), however, is that it is currently possible to simulate only a very short time period, on the order of 1 ns, so the forces needed to cause unfolding are orders of magnitude higher (∼2000 pN) than those observed in the corresponding experiments.

In the case of filamin A (previously known as ABP-280), the molecular structure is particularly interesting and may be an essential element in cytoskeletal stiffness. Filamin A is a homodimer that is joined at its subunits' C-terminal domains and that binds with actin, at the end of an extended rod region comprised largely of Ig domains similar to those in titin, to an N-terminal domain. Because of the conformation of the protein and the nature of its binding to actin, filamin A tends to form an isotropic matrix, especially in fibroblasts and macrophages, with actin filaments crossing at nearly right angles. Another important feature of filamin A

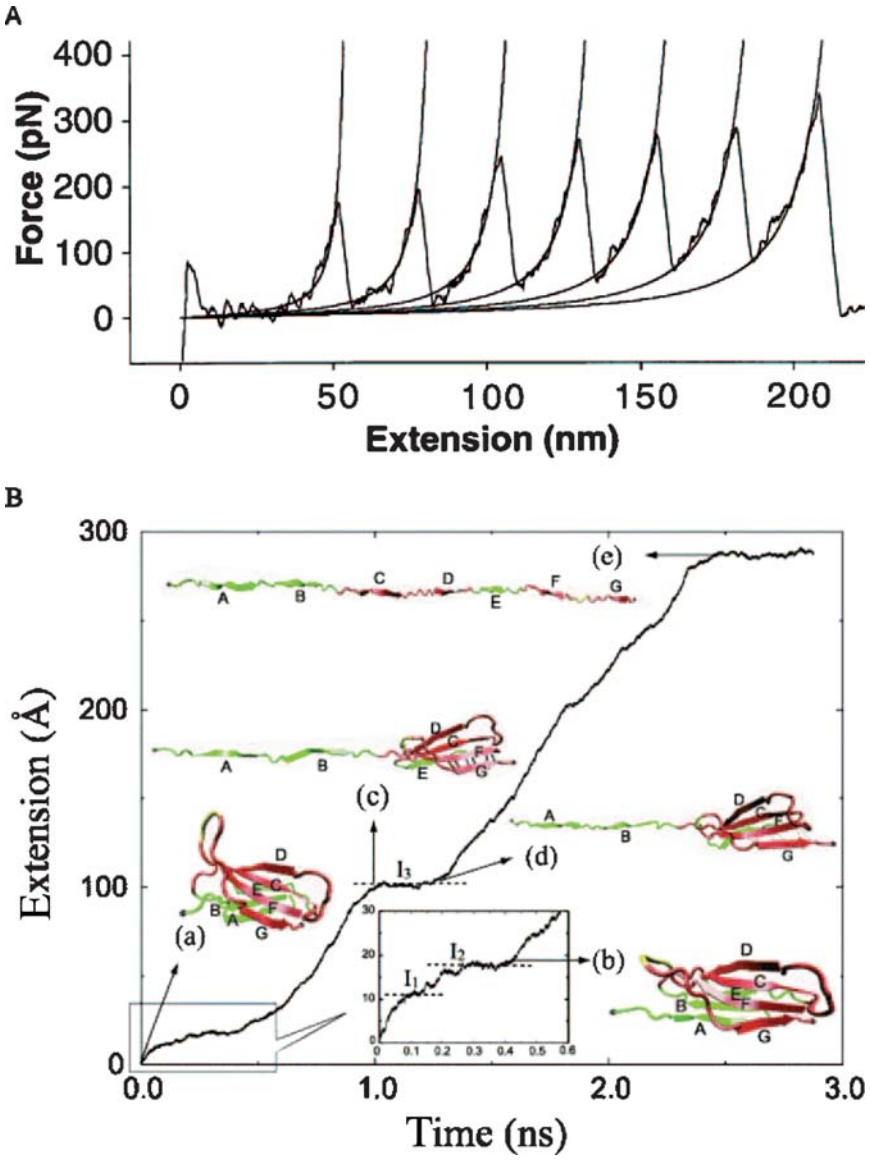

Figure 7 Stretching a single molecule. (*A*) The "sawtooth" pattern exhibited when a single fragment of titin (Ig8) is pulled using an AFM probe and plotting applied force against protein extension. Smooth lines show agreement of each segment of the curve to the worm-like chain model equation. From Reference 182. (*B*) A plot of extension against time obtained by steered molecular dynamics simulation of a single fibronectin domain when pulled at a constant force of 500 pN. Sketches show the conformations that are observed at different stages of domain unfolding from its native state (*a*) to the completely extended state (*e*). From Reference 194.

is a flexible hinge domain located about halfway along each of the two "legs" of the dimer.

Experimental measurements on single filamin A proteins exhibit the same sawtooth force-displacement character found initially with titin (Figure 7*A*), with domain unfolding occurring at a force in the range of 50–220 pN depending on the rate of pulling (189). Because these domains can reversibly refold when the force is relaxed, this unfolding/refolding process constitutes a means by which two cross-linked actin filaments can slide some distance relative to each other, yet remain bound so that they can spring back to their original position when the force is released. The role of the hinged domain has not yet been elucidated, but it, too, likely contributes to the unique characteristics of CSK elasticity.

Coupled with knowledge of the protein structure, these experimental results can provide enormous insight into the molecular basis for elastic behavior. Although a high-resolution structure of the entire filamin A (which can be obtained either by X-ray crystallography or NMR spectroscopy) has not yet been published, we do know the structure of some of the individual Ig domains (190) and can use the method of SMD to simulate the unfolding process. This has been done for titin (184), fibronectin (194), and spectrin (191), but not yet for filamin, thus allowing for the identification of the individual molecular bonds that essentially provide the glue holding the protein together and that ultimately rupture, allowing the domain to unfold. SMD has also been used to demonstrate that forces can expose cryptic, or inaccessible, binding sites, leading, in the case of fibronectin for example, to filament bundling and strengthening of the fibronectin matrix as a direct consequence of applied stress. These experimental results also provide insight into the molecular basis for frictional behavior and the structural damping law; a sawtooth force extension curve (Figure 7*A*) implies that energy dissipated upon rupture is tightly coupled to the elastic strain energy stored prior to rupture (61).

CONCLUDING PERSPECTIVE

With knowledge of the elastic character of each of the constituent proteins, one can now envision constructing a model that incorporates both the elastic properties of the individual proteins (e.g., actin and its cross-linker, filamin A) and their geometrical arrangements. In cross-linked actin gels, for example, actin filaments behave as a collection of entropic springs at low cross-link densities, but their enthalpic or mechanical stiffness (e.g., bending and extensional stiffness) becomes increasingly important with increased cross-linking and filament bundling into stress fibers. As with filamin A, actin filament elasticity is determined by the protein conformation and intermolecular bonds, giving rise to an effective elastic modulus of approximately 1.8 GPa (192). Microstructural models that incorporate these characteristics, not simply those of the CSK but also those of the extracellular matrix, are just now beginning to be developed (120), but this field will certainly grow along with our knowledge of molecular structure and our computational

capacity for molecular dynamics simulation. Similarly, molecular-level models for protein conformational change and the consequent changes in binding affinity or kinase activity will soon be developed.

In this review we have emphasized the pathway for force transmission from organ to molecule and shown evidence to suggest that even at the smallest scales, physical forces serve to distend the CSK, drive cytoskeletal remodeling, expose cryptic binding domains, and ultimately modulate reaction rates and gene expression. Evidence has now accumulated suggesting that multiscale phenomena span these scales and govern integrative lung behavior, but it is important to recognize that a sequence of reductionist models, each at a different scale and piled one upon the next, does not necessarily add up to a multiscale model or a multiscale phenomenon. Multiscale phenomena are those that intrinsically span scales; prime examples are symmorphosis, elastic similarity, structural damping, Murray's law, and glassy dynamics. Each of these represents an integrative biological phenomenon whose molecular basis remains largely unknown.

ACKNOWLEDGMENTS

We gratefully acknowledge support from grants HL33009, HL65960, HL59682, and HL64858 from the National Heart, Lung, and Blood Institute.

The *Annual Review of Physiology* is online at http://physiol.annualreviews.org

LITERATURE CITED

1. Mead J. 1973. Respiration: pulmonary mechanics. *Annu. Rev. Physiol.* 35:169–92
2. Otis AB. 1983. A perspective of respiratory mechanics. *J. Appl. Physiol.* 54: 1183–87
3. Stamenovic D. 1990. Micromechanical foundations of pulmonary elasticity. *Physiol. Rev.* 70:1117–34
4. Weibel E. 1984. *The Pathway for Oxygen*. Cambridge, MA: Harvard University Press. 425 pp.
5. Gump A, Haughney L, Fredberg J. 2001. Relaxation of activated airway smooth muscle: relative potency of isoproterenol vs. tidal stretch. *J. Appl. Physiol.* 90:2306–10
6. Weibel ER, Taylor CR, Hoppeler H. 1991. The concept of symmorphosis: a testable hypothesis of structure-function relationship. *Proc. Natl. Acad. Sci. USA* 88:10357–61
7. Weibel ER, Taylor CR, Hoppeler H. 1992. Variations in function and design: testing symmorphosis in the respiratory system. *Respir. Physiol.* 87:325–48
8. Schmidt-Nielson K. 1984. *Scaling: Why Is Animal Size So Important?* New York: Cambridge Univ. Press. 241 pp.
9. McMahon TA. 1984. *Muscles, Reflexes, and Locomotion*. Princeton, NJ: Princeton Univ. Press. 331 pp.
10. Mead J, Takishima T, Leith D. 1970. Stress distribution in lungs: a model of pulmonary elasticity. *J. Appl. Physiol.* 28: 596–608
11. Kimmel E, Kamm RD, Shapiro AH. 1987. A cellular model of lung elasticity. *J. Biomech. Eng.* 109:126–31
12. Kimmel E, Budiansky B. 1990. Surface

tension and the dodecahedron model for lung elasticity. *J. Biomech. Eng.* 112:160–67
13. Wilson TA, Bachofen H. 1982. A model for mechanical structure of the alveolar duct. *J. Appl. Physiol.* 52:1064–70
14. Lai-Fook SJ, Wilson TA, Hyatt RE, Rodarte JR. 1976. Elastic constants of inflated lobes of dog lungs. *J. Appl. Physiol.* 40:508–13
15. Boriek AM, Wilson TA, Rodarte JR. 1994. Displacements and strains in the costal diaphragm of the dog. *J. Appl. Physiol.* 76:223–29
16. Boriek AM, Liu S, Rodarte JR. 1993. Costal diaphragm curvature in the dog. *J. Appl. Physiol.* 75:527–33
17. Macklem PT, Macklem DM, De Troyer A. 1983. A model of inspiratory muscle mechanics. *J. Appl. Physiol.* 55:547–57
18. Loring SH, Mead J. 1982. Action of the diaphragm on the rib cage inferred from a force-balance analysis. *J. Appl. Physiol.* 53:756–60
19. Sprung J, Deschamps C, Hubmayr RD, Walters BJ, Rodarte JR. 1989. In vivo regional diaphragm function in dogs. *J. Appl. Physiol.* 67:655–62
20. Faridy EE, Kidd R, Milic-Emili J. 1967. Topographical distribution of inspired gas in excised lobes of dogs. *J. Appl. Physiol.* 22:760–66
21. Milic-Emili J, Henderson JA, Dolovich MB, Trop D, Kaneko K. 1966. Regional distribution of inspired gas in the lung. *J. Appl. Physiol.* 21:749–59
22. Hoppin FG Jr, Green ID, Mead J. 1969. Distribution of pleural surface pressure in dogs. *J. Appl. Physiol.* 27:863–73
23. Hajji MA, Wilson TA, Lai-Fook SJ. 1979. Improved measurements of shear modulus and pleural membrane tension of the lung. *J. Appl. Physiol.* 47:175–81
24. Kallok MJ, Lai-Fook SJ, Hajji MA, Wilson TA. 1983. Axial distortion of airways in the lung. *J. Appl. Physiol.* 54:185–90
25. Lai-Fook SJ. 1979. A continuum mechanics analysis of pulmonary vascular interdependence in isolated dog lobes. *J. Appl. Physiol.* 46:419–29
26. Lai-Fook SJ. 1981. Elasticity analysis of lung deformation problems. *Ann. Biomed. Eng.* 9:451–62
27. Lai-Fook SJ, Hyatt RE. 1979. Effect of parenchyma and length changes on vessel pressure-diameter behavior in pig lungs. *J. Appl. Physiol.* 47:666–69
28. Lai-Fook SJ, Hyatt RE, Rodarte JR. 1978. Effect of parenchymal shear modulus and lung volume on bronchial pressure-diameter behavior. *J. Appl. Physiol.* 44: 859–68
29. Lai-Fook SJ, Kallok MJ. 1982. Bronchial-arterial interdependence in isolated dog lung. *J. Appl. Physiol.* 52:1000–7
30. Oldmixon EH, Hoppin FG Jr. 1984. Comparison of amounts of collagen and elastin in pleura and parenchyma of dog lung. *J. Appl. Physiol.* 56:1383–88
31. Oldmixon EH, Carlsson K, Kuhn C 3rd, Butler JP, Hoppin FG Jr. 2001. α-actin: disposition, quantities, and estimated effects on lung recoil and compliance. *J. Appl. Physiol.* 91:459–73
32. Otis AB, McKerrow CB, Bartlett RA, Mead J, McIlroy MB, et al. 1956. Mechanical factors in distribution of pulmonary ventilation. *J. Appl. Physiol.* 8:427–43
33. Engel LA, Landau L, Taussig L, Martin RR, Sybrecht G. 1976. Influence of bronchomotor tone on regional ventilation distribution at residual volume. *J. Appl. Physiol.* 40:411–16
34. Crawford AB, Cotton DJ, Paiva M, Engel LA. 1989. Effect of lung volume on ventilation distribution. *J. Appl. Physiol.* 66:2502–10
35. Wagner PD, Saltzman HA, West JB. 1974. Measurement of continuous distributions of ventilation-perfusion ratios: theory. *J. Appl. Physiol.* 36:588–99
36. Wagner PD, Laravuso RB, Uhl RR, West JB. 1974. Continuous distributions of ventilation-perfusion ratios in normal subjects breathing air and 100 per cent O2. *J. Clin. Invest.* 54:54–68

37. Mead J, Turner JM, Macklem PT, Little JB. 1967. Significance of the relationship between lung recoil and maximum expiratory flow. *J. Appl. Physiol.* 22:95–108
38. Hubmayr RD, Walters BJ, Chevalier PA, Rodarte JR, Olson LE. 1983. Topographical distribution of regional lung volume in anesthetized dogs. *J. Appl. Physiol.* 54:1048–56
39. West JB, Dollery CT. 1960. Distribution of blood flow and ventilation-perfusion ratio in the lung, measured with radioactive carbon dioxide. *J. Appl. Physiol.* 15: 405–10
40. West JB, Dollery CT, Naimark A. 1964. Distribution of blood flow in isolated lung; relation to vascular and alveolar pressures. *J. Appl. Physiol.* 19:713–24
41. Hughes JM, Glazier JB, Maloney JE, West JB. 1968. Effect of lung volume on the distribution of pulmonary blood flow in man. *Respir. Physiol.* 4:58–72
42. Permutt S, Bromberger-Barnea B, Bane HN. 1962. Alveolar pressure, pulmonary venous pressure, and the vascular waterfall. *Med. Thorac.* 19:239–60
43. Skloot G, Permutt S, Togias A. 1995. Airway hyperresponsiveness in asthma: a problem of limited smooth muscle relaxation with inspiration. *J. Clin. Invest.* 96:2393–403
44. Hoppin FG Jr, Lee GC, Dawson SV. 1975. Properties of lung parenchyma in distortion. *J. Appl. Physiol.* 39:742–51
45. Sasaki H, Hoppin FG Jr, Takishima T. 1978. Peribronchial pressure in excised dog lungs. *J. Appl. Physiol.* 45:858–69
46. Elad D, Kamm RD, Shapiro AH. 1988. Tube law for the intrapulmonary airway. *J. Appl. Physiol.* 65:7–13
47. Mortola JP, Rossi A, Zocchi L. 1984. Pressure-volume curve of lung and lobes in kittens. *J. Appl. Physiol.* 56:948–53
48. Stocks J. 1999. Respiratory physiology during early life. *Monaldi Arch. Chest Dis.* 54:358–64
49. Shen X, Ramchandani R, Dunn B, Lambert R, Gunst SJ, Tepper RS. 2000. Effect of transpulmonary pressure on airway diameter and responsiveness of immature and mature rabbits. *J. Appl. Physiol.* 89:1584–90
50. Schroter RC. 1980. Quantitative comparisons of mammalian lung pressure volume curves. *Respir. Physiol.* 42:101–7
51. Mercer RR, Russell ML, Crapo JD. 1994. Alveolar septal structure in different species. *J. Appl. Physiol.* 77:1060–66
52. Agostoni E, D'Angelo E. 1970. Comparative features of the transpulmonary pressure. *Respir. Physiol.* 11:76–83
53. Bachofen H, Hildebrandt J, Bachofen M. 1970. Pressure-volume curves of air- and liquid-filled excised lungs-surface tension in situ. *J. Appl. Physiol.* 29:422–31
54. Bachofen H, Schurch S, Urbinelli M, Weibel ER. 1987. Relations among alveolar surface tension, surface area, volume, and recoil pressure. *J. Appl. Physiol.* 62:1878–87
55. Tenney SM, Remmers JE. 1963. Comparative quantitative morphology of the mammalian lung: diffusing area. *Nature* 197:54–56
56. Ludwig MS, Dreshaj I, Solway J, Munoz A, Ingram RH Jr. 1987. Partitioning of pulmonary resistance during constriction in the dog: effects of volume history. *J. Appl. Physiol.* 62:807–15
57. Peslin R, Fredberg J. 1986. Oscillation mechanics of the respiratory system. In *Handbook of Physiology: The Respiratory System III, Respiration*, PT Macklem, J Mead, eds, pp. 145–77. Bethesda, MD: Am. Physiol. Soc.
58. Ludwig MS, Robatto FM, Simard S, Stamenovic D, Fredberg JJ. 1992. Lung tissue resistance during contractile stimulation: structural damping decomposition. *J. Appl. Physiol.* 72:1332–37
59. Nagase T, Dallaire MJ, Ludwig MS. 1996. Airway and tissue behavior during early response in sensitized rats: role of 5-HT and LTD4. *J. Appl. Physiol.* 80:583–90
60. Jensen A, Atileh H, Suki B, Ingenito EP, Lutchen KR. 2001. Airway caliber in

healthy and asthmatic subjects: effects of bronchial challenge and deep inspirations. *J. Appl. Physiol.* 91:506–15
61. Fredberg JJ, Stamenovic D. 1989. On the imperfect elasticity of lung tissue. *J. Appl. Physiol.* 67:2408–19
62. Bayliss L, Robertson G. 1939. The visco-elastic properties of the lungs. *Q. J. Exp. Physiol.* 29:27–47
63. Hildebrandt J. 1969. Comparison of mathematical models for cat lung and viscoelastic balloon derived by Laplace transform methods from pressure-volume data. *Bull. Math Biophys.* 31:651–67
64. Hantos Z, Daroczy B, Suki B, Nagy S, Fredberg JJ. 1992. Input impedance and peripheral inhomogeneity of dog lungs. *J. Appl. Physiol.* 72:168–78
65. Fredberg JJ, Bunk D, Ingenito E, Shore SA. 1993. Tissue resistance and the contractile state of lung parenchyma. *J. Appl. Physiol.* 74:1387–97
66. Fredberg JJ, Jones KA, Nathan M, Raboudi S, Prakash YS, et al. 1996. Friction in airway smooth muscle: mechanism, latch, and implications in asthma. *J. Appl. Physiol.* 81:2703–12
67. Fabry B, Maksym GN, Butler JP, Glogauer M, Navajas D, Fredberg JJ. 2001. Scaling the microrheology of living cells. *Phys. Rev. Lett.* 87:148102
68. Fabry B, Maksym GN, Butler JP, Glogauer M, Navajas D, et al. 2003. Time scale and other invariants of integrative mechanical behavior in living cells. *Phys. Rev. E Stat. Nonlin. Soft Matter Phys.* 68:041914
69. Fabry B, Maksym GN, Shore SA, Moore PE, Panettieri RA Jr, et al. 2001. Time course and heterogeneity of contractile responses in cultured human airway smooth muscle cells. *J. Appl. Physiol.* 91:986–94
70. Crandal S. 1970. The role of damping in vibration theory. *J. Sound Vibrat.* 11:3–18
71. Fung Y. 1988. *Biomechanics: Mechanical Properties of Living Tissues*. New York: Springer-Verlag. 433 pp.
72. Hubmayr RD. 2000. Biology lessons from oscillatory cell mechanics. *J. Appl. Physiol.* 89:1617–18
73. Murray C. 1926. The physiological principle of minimum work. I. The vascular system and the cost of blood volume. *Proc. Natl. Acad. Sci. USA* 12:207–14
74. McCulloh KA, Sperry JS, Adler FR. 2003. Water transport in plants obeys Murray's law. *Nature* 421:939–42
75. Chien S, Shyy JY. 1998. Effects of hemodynamic forces on gene expression and signal transduction in endothelial cells. *Biol. Bull.* 194:390–91
76. Nollert MU, Panaro NJ, McIntire LV. 1992. Regulation of genetic expression in shear stress-stimulated endothelial cells. *Ann. NY Acad. Sci.* 665:94–104
77. Bershadsky AD, Balaban NQ, Geiger B. 2003. Adhesion-dependent cell mechanosensitivity. *Annu. Rev. Cell. Dev. Biol.* 19:677–95
78. Geiger B, Bershadsky A, Pankov R, Yamada KM. 2001. Transmembrane crosstalk between the extracellular matrix–cytoskeleton crosstalk. *Nat. Rev. Mol. Cell Biol.* 2:793–805
79. Saez AO, Zhang W, Wu Y, Turner CE, Tang DD, Gunst SJ. 2004. Tension development during contractile stimulation of smooth muscle requires recruitment of paxillin and vinculin to the membrane. *Am. J. Physiol. Cell Physiol.* 286:C433–47
80. Tang DD, Wu MF, Opazo Saez AM, Gunst SJ. 2002. The focal adhesion protein paxillin regulates contraction in canine tracheal smooth muscle. *J. Physiol.* 542:501–13
81. Davies PF, Barbee KA, Volin MV, Robotewskyj A, Chen J, et al. 1997. Spatial relationships in early signaling events of flow-mediated endothelial mechanotransduction. *Annu. Rev. Physiol.* 59:527–49
82. Stamenovic D, Ingber DE. 2002. Models of cytoskeletal mechanics of adherent cells. *Biomech. Model. Mechanobiol.* 1:95–108

83. Stamenovic D, Fredberg JJ, Wang N, Butler JP, Ingber DE. 1996. A microstructural approach to cytoskeletal mechanics based on tensegrity. *J. Theor. Biol.* 181:125–36
84. Stamenovic D, Mijailovich SM, Tolic-Norrelykke IM, Chen J, Wang N. 2002. Cell prestress. II. Contribution of microtubules. *Am. J. Physiol. Cell Physiol.* 282:C617–24
85. Cukierman E, Pankov R, Stevens DR, Yamada KM. 2001. Taking cell-matrix adhesions to the third dimension. *Science* 294:1708–12
86. Geiger B. 2001. Cell biology. Encounters in space. *Science* 294:1661–63
87. Balaban NQ, Schwarz US, Riveline D, Goichberg P, Tzur G, et al. 2001. Force and focal adhesion assembly: a close relationship studied using elastic micropatterned substrates. *Nat. Cell Biol.* 3:466–72.
88. Zamir E, Katz M, Posen Y, Erez N, Yamada KM, et al. 2000. Dynamics and segregation of cell-matrix adhesions in cultured fibroblasts. *Nat. Cell Biol.* 2:191–96
89. Weichselbaum M, Sparrow MP. 1999. A confocal microscopic study of the formation of ganglia in the airways of fetal pig lung. *Am. J. Respir. Cell. Mol. Biol.* 21:607–20
90. Sparrow MP, Weichselbaum M, McCray PB. 1999. Development of the innervation and airway smooth muscle in human fetal lung. *Am. J. Respir. Cell. Mol. Biol.* 20:550–60
91. Seow CY, Fredberg JJ. 2001. Historical perspective on airway smooth muscle: the saga of a frustrated cell. *J. Appl. Physiol.* 91:938–52
92. Dembo M, Wang YL. 1999. Stresses at the cell-to-substrate interface during locomotion of fibroblasts. *Biophys. J.* 76:2307–16
93. Butler JP, Tolic-Norrelykke IM, Fabry B, Fredberg JJ. 2002. Traction fields, moments, and strain energy that cells exert on their surroundings. *Am. J. Physiol. Cell Physiol.* 282:C595–605
94. Schwarz US, Balaban NQ, Riveline D, Bershadsky A, Geiger B, Safran SA. 2002. Calculation of forces at focal adhesions from elastic substrate data: the effect of localized force and the need for regularization. *Biophys. J.* 83:1380–94
95. Tolic-Norrelykke IM, Butler JP, Chen J, Wang N. 2002. Spatial and temporal traction response in human airway smooth muscle cells. *Am. J. Physiol. Cell Physiol.* 283:C1254–66
96. Wang N, Tolic-Norrelykke IM, Chen J, Mijailovich SM, Butler JP, et al. 2002. Cell prestress. I. Stiffness and prestress are closely associated in adherent contractile cells. *Am. J. Physiol. Cell Physiol.* 282:C606–16
97. An SS, Pennella CM, Gonnabathula A, Chen J, Wang N, et al. 2005. Hypoxia alters biophysical properties of endothelial cells via p38 MAPK-and Rho kinase-dependent pathways. *Am. J. Physiol. Cell Physiol.* 289:C521–30
98. du Roure O, Saez A, Buguin A, Austin RH, Chavrier P, et al. 2005. Force mapping in epithelial cell migration. *Proc. Natl. Acad. Sci. USA* 102:2390–95
99. Glogauer M, Arora P, Chou D, Janmey PA, Downey GP, McCulloch CA. 1998. The role of actin-binding protein 280 in integrin-dependent mechanoprotection. *J. Biol. Chem.* 273:1689–98
100. Giannone G, Jiang G, Sutton DH, Critchley DR, Sheetz MP. 2003. Talin1 is critical for force-dependent reinforcement of initial integrin-cytoskeleton bonds but not tyrosine kinase activation. *J. Cell Biol.* 163:409–19
101. Panettieri RA, Murray RK, DePalo LR, Yadvish PA, Kotlikoff MI. 1989. A human airway smooth muscle cell line that retains physiological responsiveness. *Am. J. Physiol.* 256:C329–35
102. Stamenovic D, Wilson TA. 1992. Parenchymal stability. *J. Appl. Physiol.* 73:596–602
103. Lambert RK, Wilson TA. 1973. A model for the elastic properties of the lung and

their effect of expiratory flow. *J. Appl. Physiol.* 34:34–48

104. Stamenovic D, Wilson TA. 1985. A strain energy function for lung parenchyma. *J. Biomech. Eng.* 107:81–86
105. Stamenovic D, Coughlin MF. 1999. The role of prestress and architecture of the cytoskeleton and deformability of cytoskeletal filaments in mechanics of adherent cells: a quantitative analysis. *J. Theor. Biol.* 201:63–74
106. Stamenovic D, Liang Z, Chen J, Wang N. 2002. Effect of the cytoskeletal prestress on the mechanical impedance of cultured airway smooth muscle cells. *J. Appl. Physiol.* 92:1443–50
107. Pourati J, Maniotis A, Spiegel D, Schaffer JL, Butler JP, et al. 1998. Is cytoskeletal tension a major determinant of cell deformability in adherent endothelial cells? *Am. J. Physiol.* 274:C1283–89
108. Wang N, Naruse K, Stamenovic D, Fredberg JJ, Mijailovich SM, et al. 2001. Mechanical behavior in living cells consistent with the tensegrity model. *Proc. Natl. Acad. Sci. USA* 98:7765–70
109. Griffin MA, Engler AJ, Barber TA, Healy KE, Sweeney HL, Discher DE. 2004. Patterning, prestress, and peeling dynamics of myocytes. *Biophys. J.* 86:1209–22
110. Budiansky B, Kimmel E. 1987. Elastic moduli of lungs. *J. Appl. Mech.* 54S:351–58
111. Heidemann SR, Lamoureaux P, Buxbaum RE. 2000. Opposing views on tensegrity as a structural framework for understanding cell mechanics. *J. Appl. Physiol.* 89:1670–78
112. Ingber DE. 2000. Opposing views on tensegrity as a structural framework for understanding cell mechanics. *J. Appl. Physiol.* 89:1663–70
113. Ingber DE. 1998. The architecture of life. *Sci. Am.* 278:48–57
114. Wang N, Butler JP, Ingber DE. 1993. Mechanotransduction across the cell surface and through the cytoskeleton. *Science* 260:1124–27
115. Wang N, Ingber DE. 1994. Control of cytoskeletal mechanics by extracellular matrix, cell shape, and mechanical tension. *Biophys. J.* 66:2181–89
116. Wang N, Ostuni E, Whitesides GM, Ingber DE. 2002. Micropatterning tractional forces in living cells. *Cell Motil. Cytoskeleton* 52:97–106
117. Parker KK, Brock AL, Brangwynne C, Mannix RJ, Wang N, et al. 2002. Directional control of lamellipodia extension by constraining cell shape and orienting cell tractional forces. *FASEB J.* 16:1195–204
118. MacKintosh FC, Käs J, Janmey PA. 1995. Elasticity of semiflexible biopolymer networks. *Phys. Rev. Lett.* 75:4425–28
119. Gardel ML, Shin JH, MacKintosh FC, Mahadevan L, Matsudaira PA, Weitz DA. 2004. Scaling of F-actin network rheology to probe single filament elasticity and dynamics. *Phys. Rev. Lett.* 93:188102
120. Gardel ML, Shin JH, MacKintosh FC, Mahadevan L, Matsudaira P, Weitz DA. 2004. Elastic behavior of cross-linked and bundled actin networks. *Science* 304:1301–5
121. Mahaffy RE, Shih CK, MacKintosh FC, Kas J. 2000. Scanning probe-based frequency-dependent microrheology of polymer gels and biological cells. *Phys. Rev. Lett.* 85:880–83
122. Gittes F, MacKintosh FC. 1998. Dynamic shear modulus of a semiflexible polymer network. *Phys. Rev. E* 58:R1241–44
123. Head DA, Levine AJ, MacKintosh FC. 2003. Deformation of cross-linked semiflexible polymer networks. *Phys. Rev. Lett.* 91:108102
124. Hu S, Chen J, Fabry B, Numaguchi Y, Gouldstone A, et al. 2003. Intracellular stress tomography reveals stress focusing and structural anisotropy in cytoskeleton of living cells. *Am. J. Physiol. Cell Physiol.* 285:C1082–90
125. Maniotis AJ, Chen CS, Ingber DE. 1997. Demonstration of mechanical connections between integrins, cytoskeletal filaments, and nucleoplasm that stabilize

nuclear structure. *Proc. Natl. Acad. Sci. USA* 94:849–54
126. Hu S, Eberhard L, Chen J, Love JC, Butler JP, et al. 2004. Mechanical anisotropy of adherent cells probed by a 3D magnetic twisting device. *Am. J. Physiol. Cell Physiol.* 287:1184–91
127. Dahl KN, Engler AJ, Pajerowski JD, Discher DE. 2005. Power-law rheology of isolated nuclei with deformation mapping of nuclear sub-structures. *Biophys. J.* 89(4):2855–64, 2005
128. Bursac P, Lenormand G, Fabry B, Oliver M, Weitz DA, et al. 2005. Cytoskeletal remodelling and slow dynamics in the living cell. *Nat. Mat.* 4:557–71
129. Seow C. 2005. Fashionable glass. *Nature* 435:1172–73
130. Puig-De-Morales M, Millet E, Fabry B, Navajas D, Wang N, et al. 2004. Cytoskeletal mechanics in the adherent human airway smooth muscle cell: probe specificity and scaling of protein-protein dynamics. *Am. J. Physiol. Cell Physiol.* 287:C643–54
131. Lenormand G, Millet E, Fabry B, Butler J, Fredberg J. 2004. Linearity and time-scale invariance of the creep function in living cells. *J. Roy. Soc. Interface* 1:91–97
132. Alcaraz J, Buscemi L, Grabulosa M, Trepat X, Fabry B, et al. 2003. Microrheology of human lung epithelial cells measured by atomic force microscopy. *Biophys. J.* 84:2071–79
133. Balland M, Richert A, Gallet F. 2005. The dissipative contribution of myosin II in the cytoskeleton dynamics of myoblasts. *Eur. Biophys. J.* 34:255–61
134. Desprat N, Richert A, Simeon J, Asnacios A. 2005. Creep function of a single living cell. *Biophys. J.* 88:2224–33
135. Fabry B, Fredberg JJ. 2003. Remodeling of the airway smooth muscle cell: are we built of glass? *Respir. Physiol. Neurobiol.* 137:109–24
136. Sollich P. 1998. Rheological constitutive equation for a model of soft glassy materials. *Physiol. Rev.* 58:738–59
137. Sollich P, Lequeux F, Hebraud P, Cates ME. 1997. Rheology of soft glassy mateirals. *Phys. Rev. Lett* 78:2020–23
138. Gunst SJ, Fredberg JJ. 2003. The first three minutes: smooth muscle contraction, cytoskeletal events, and soft glasses. *J. Appl. Physiol.* 95:413–25
139. Howard J. 2001. *Mechanics of Motor Proteins and the Cytoskeleton*. Sunderland, MA: Sinauer. 367 pp.
140. Trappe V, Prasad V, Cipelletti L, Segre PN, Weitz DA. 2001. Jamming phase diagram for attractive particles. *Nature* 411:772–75
141. Segre PN, Prasad V, Schofield AB, Weitz DA. 2001. Glasslike kinetic arrest at the colloidal-gelation transition. *Phys. Rev. Lett.* 86:6042–45
142. Ellis RJ, Minton AP. 2003. Cell biology: join the crowd. *Nature* 425:27–28
143. Ellis RJ. 2001. Macromolecular crowding: obvious but underappreciated. *Trends Biochem. Sci.* 26:597–604
144. Ellis RJ. 2001. Macromolecular crowding: an important but neglected aspect of the intracellular environment. *Curr. Opin. Struct. Biol.* 11:114–19
145. Pollack GH. 2001. *Cells, Gels and the Engines of Life*. Seattle, WA: Ebner. 305 pp.
146. Goodsell D. 2000. Biomolecules and nanotechnology. *Am. Sci.* 88:230–37
147. Dobson CM. 2004. Chemical space and biology. *Nature* 432:824–28
148. Mehta D, Gunst SJ. 1999. Actin polymerization stimulated by contractile activation regulates force development in canine tracheal smooth muscle. *J. Physiol.* 519(Pt. 3):829–40
149. Trepat X, Grabulosa M, Puig F, Maksym GN, Navajas D, Farre R. 2004. Viscoelasticity of human alveolar epithelial cells subjected to stretch. *Am. J. Physiol. Lung Cell Mol. Physiol.* 287:L1025–34
150. Stamenovic D, Suki B, Fabry B, Wang N, Fredberg JJ. 2004. Rheology of airway smooth muscle cells is associated with cytoskeletal contractile stress. *J. Appl. Physiol.* 96:1600–5

151. Davies PF, Robotewskyj A, Griem ML. 1994. Quantitative studies of endothelial cell adhesion. Directional remodeling of focal adhesion sites in response to flow forces. *J. Clin. Invest.* 93:2031–38
152. Hamill OP, Martinac B. 2001. Molecular basis of mechanotransduction in living cells. *Physiol. Rev.* 81:685–740
153. Fisher JL, Margulies SS. 2002. Na^+-K^+-ATPase activity in alveolar epithelial cells increases with cyclic stretch. *Am. J. Physiol. Lung Cell Mol. Physiol.* 283:L737–46
154. Gullingsrud J, Kosztin D, Schulten K. 2001. Structural determinants of MscL gating studied by molecular dynamics simulations. *Biophys. J.* 80:2074–81
155. Gullingsrud J, Schulten K. 2003. Gating of MscL studied by steered molecular dynamics. *Biophys. J.* 85:2087–99
156. Dreyfuss D, Martin-Lefevre L, Saumon G. 1999. Hyperinflation-induced lung injury during alveolar flooding in rats: effect of perfluorocarbon instillation. *Am. J. Respir. Crit. Care Med.* 159:1752–57
157. Dreyfuss D, Saumon G. 1998. Ventilator-induced lung injury: lessons from experimental studies. *Am. J. Respir. Crit. Care Med.* 157:294–323
158. Tschumperlin DJ, Margulies SS. 1999. Alveolar epithelial surface area-volume relationship in isolated rat lungs. *J. Appl. Physiol.* 86:2026–33
159. Chapman KE, Sinclair SE, Zhuang D, Hassid A, Desai L, Waters CM. 2005. Cyclic mechanical strain increases reactive oxygen species production in pulmonary epithelial cells. *Am. J. Physiol. Lung Cell Mol. Physiol.* 289:834–41
160. Wilson MR, Choudhury S, Goddard ME, O′Dea KP, Nicholson AG, Takata M. 2003. High tidal volume upregulates intrapulmonary cytokines in an in vivo mouse model of ventilator-induced lung injury. *J. Appl. Physiol.* 95:1385–93
161. Choudhury S, Wilson MR, Goddard ME, O′Dea KP, Takata M. 2004. Mechanisms of early pulmonary neutrophil sequestration in ventilator-induced lung injury in mice. *Am. J. Physiol. Lung Cell Mol. Physiol.* 287:L902–10
162. Ali MH, Pearlstein DP, Mathieu CE, Schumacker PT. 2004. Mitochondrial requirement for endothelial responses to cyclic strain: implications for mechanotransduction. *Am. J. Physiol. Lung Cell Mol. Physiol.* 287:L486–96
163. Ichimura H, Parthasarathi K, Quadri S, Issekutz AC, Bhattacharya J. 2003. Mechano-oxidative coupling by mitochondria induces proinflammatory responses in lung venular capillaries. *J. Clin. Invest.* 111:691–99
164. Jiang G, Giannone G, Critchley DR, Fukumoto E, Sheetz MP. 2003. Two-piconewton slip bond between fibronectin and the cytoskeleton depends on talin. *Nature* 424:334–37
165. Evans E. 2001. Probing the relation between force—lifetime–and chemistry in single molecular bonds. *Annu. Rev. Biophys. Biomol. Struct.* 30:105–28
166. Sawada Y, Sheetz MP. 2002. Force transduction by Triton cytoskeletons. *J. Cell Biol.* 156:609–15
167. Wang Y, Botvinick EL, Zhao Y, Berns MW, Usami S, et al. 2005. Visualizing the mechanical activation of Src. *Nature* 434:1040–45
168. Zhong C, Chrzanowska-Wodnicka M, Brown J, Shaub A, Belkin AM, Burridge K. 1998. Rho-mediated contractility exposes a cryptic site in fibronectin and induces fibronectin matrix assembly. *J. Cell Biol.* 141:539–51
169. Gilmore AP, Burridge K. 1995. Cell adhesion. Cryptic sites in vinculin. *Nature* 373:197
170. Sampath R, Gallagher PJ, Pavalko FM. 1998. Cytoskeletal interactions with the leukocyte integrin beta2 cytoplasmic tail. Activation-dependent regulation of associations with talin and alpha-actinin. *J. Biol. Chem.* 273:33588–94
171. Papagrigoriou E, Gingras AR, Barsukov IL, Bate N, Fillingham IJ, et al. 2004. Activation of a vinculin-binding site in the

talin rod involves rearrangement of a five-helix bundle. *EMBO J.* 23:2942–51
172. Fillingham I, Gingras AR, Papagrigoriou E, Patel B, Emsley J, et al. 2005. A vinculin binding domain from the talin rod unfolds to form a complex with the vinculin head. *Structure* 13:65–74
173. Yap B, Kamm RD. 2005. Mechanical deformation of neutrophils into narrow channels induces pseudopod projection and changes in biomechanical properties. *J. Appl. Physiol.* 98:1930–39
174. Kitagawa Y, Van Eeden SF, Redenbach DM, Daya M, Walker BA, et al. 1997. Effect of mechanical deformation on structure and function of polymorphonuclear leukocytes. *J. Appl. Physiol.* 82:1397–405
175. Yap B, Kamm RD. 2005. Cytoskeletal remodeling and cellular activation during deformation of neutrophils into narrow channels. *J. Appl. Physiol.*:doi: 10.1152/japplphysiol.00503.2005. In press
176. Tschumperlin DJ, Dai G, Maly IV, Kikuchi T, Laiho LH, et al. 2004. Mechanotransduction through growth-factor shedding into the extracellular space. *Nature* 429:83–86
177. Ressler B, Lee RT, Randell SH, Drazen JM, Kamm RD. 2000. Molecular responses of rat tracheal epithelial cells to transmembrane pressure. *Am. J. Physiol. Lung Cell Mol. Physiol.* 278:L1264–72
178. Swartz MA, Tschumperlin DJ, Kamm RD, Drazen JM. 2001. Mechanical stress is communicated between different cell types to elicit matrix remodeling. *Proc. Natl. Acad. Sci. USA* 98:6180–85
179. Budhiraja R, Tuder RM, Hassoun PM. 2004. Endothelial dysfunction in pulmonary hypertension. *Circulation* 109:159–65
180. Tozzi CA, Poiani GJ, Harangozo AM, Boyd CD, Riley DJ. 1989. Pressure-induced connective tissue synthesis in pulmonary artery segments is dependent on intact endothelium. *J. Clin. Invest.* 84:1005–12
181. Strauss BH, Rabinovitch M. 2000. Adventitial fibroblasts: defining a role in vessel wall remodeling. *Am. J. Respir. Cell. Mol. Biol.* 22:1–3
182. Rief M, Gautel M, Oesterhelt F, Fernandez JM, Gaub HE. 1997. Reversible unfolding of individual titin immunoglobulin domains by AFM. *Science* 276:1109–12
183. Kellermayer MS, Smith SB, Granzier HL, Bustamante C. 1997. Folding-unfolding transitions in single titin molecules characterized with laser tweezers. *Science* 276:1112–16
184. Gao M, Lu H, Schulten K. 2002. Unfolding of titin domains studied by molecular dynamics simulations. *J. Muscle Res. Cell Motil.* 23:513–21
185. Granzier H, Labeit S. 2002. Cardiac titin: an adjustable multi-functional spring. *J. Physiol.* 541:335–42
186. Discher DE, Carl P. 2001. New insights into red cell network structure, elasticity, and spectrin unfolding–a current review. *Cell Mol. Biol. Lett.* 6:593–606
187. Furuike S, Ito T, Yamazaki M. 2001. Mechanical unfolding of single filamin A (ABP-280) molecules detected by atomic force microscopy. *FEBS Lett.* 498:72–75
188. Gao M, Lu H, Schulten K. 2001. Simulated refolding of stretched titin immunoglobulin domains. *Biophys. J.* 81: 2268–77
189. Yamazaki M, Furuike S, Ito T. 2002. Mechanical response of single filamin A (ABP-280) molecules and its role in the actin cytoskeleton. *J. Muscle Res. Cell Motil.* 23:525–34
190. Schwaiger I, Kardinal A, Schleicher M, Noegel AA, Rief M. 2004. A mechanical unfolding intermediate in an actin-crosslinking protein. *Nat. Struct. Mol. Biol.* 11:81–85
191. Ortiz V, Nielsen SO, Klein ML, Discher DE. 2005. Unfolding a linker between helical repeats. *J. Mol. Biol.* 349:638–47
192. Gittes F, Mickey B, Nettleton J, Howard

J. 1993. Flexural rigidity of microtubules and actin filaments measured from thermal fluctuations in shape. *J. Cell Biol.* 120:923–34

193. Laudadio R, Millet E, Fabry F, An S, Butler J, Fredberg J. The rat airway smooth muscle cell during actin modulation: rheology and glassy dynamics. *Am. J. Physiol. Cell Physiol.*: doi:10.1152/ajpcell.00060.2005. In press
194. Gao M, Craig D, Vogel V, Schulten K. 2002. Identifying unfolding intermediates of FN-III10 by steered molecular dynamics. *J. Mol. Biol.* 323:939–50

Annual Review of Physiology
Volume 68, 2006

CONTENTS